https://doi.org/10.1016/j.ocecoaman.2023.106809

Optimal Scheduling of Vessels Passing a Waterway Bottleneck

Xiao Yang [a], Weihua Gu [a,*], Shuaian Wang [b]

[a] Department of Electrical Engineering, The Hong Kong Polytechnic University, Hong Kong Special Administrative Region

[b] Department of Logistics & Maritime Studies, The Hong Kong Polytechnic University, Hong Kong Special Administrative Region

* Corresponding author, Email: weihua.gu@polyu.edu.hk

Abstract

We develop a novel schedule optimization model for vessels passing a waterway bottleneck. From the system-optimal perspective, the model aims to minimize the total vessel bunker cost and delay penalties at destinations by incorporating the nonlinear relationship between bunker consumption and sailing speed into its calculations. The nonlinear model is linearized via two commonly used approximation techniques. The first one linearizes the bunker consumption function using a piecewise linear lower bound, while the second does so by discretizing the time. Numerical case studies are conducted for a real-world waterway bottleneck, the Three Gorges Dam Lock. Results reveal how the optimal cost components, vessel schedules, and delays are affected by key operating parameters, including the fuel prices, delay penalty rates, and the tightness of sailing time windows. Comparison against two simpler benchmark scheduling strategies (one with no vessel coordination and the other adopting a naïve coordination) manifests the sizeable benefit of optimal vessel scheduling.

This paper presents the first investigation into the system-optimal scheduling strategy for vessels navigating a shared bottleneck, considering bunker costs, schedule delay penalties, and varying sailing speeds. The results highlight the significant potential of system-optimal scheduling and potential coordination strategies that enable approximation of the system-optimal solution. Additionally, our numerical experiments uncover the limitations of the outer-approximation method, while demonstrating that the discrete-time approach surpasses it in terms of both solution quality and computational efficiency.

Keywords: optimal ship scheduling; waterway bottleneck; piecewise linear approximation; discrete-time approximation; bunker cost

1. Introduction

1.1 Background

Waterway transportation (including both seaborne and river-borne transportation) plays a vital role in the global economy. Over 80% of the international trade in goods (approximately 11.1 billion tons in 2019) is carried by waterways (UNCTAD, 2020). This number increased at an average annual rate of 2.8% before the COVID-19 outbreak (WTO, 2021).

The shipping industry's rapid growth has led to severe vessel congestion at waterway bottlenecks, including busy dams, locks, canals, and terminals (Feng et al., 2015, 2020; Huang et al., 2022; Lin et al., 2022). For instance, cargo ships can experience up to 3-day wait times at the Three Gorges Dam (TGD) on the Yangtze River during peak seasons (Zhao et al., 2020).

In Spring 2021, due to surging demand, waiting times for Neopanamax and liquefied natural gas vessels transiting the Panama Canal reached 8–9 days (Connolly, 2021), resulting in substantial congestion costs (e.g., the daily cost of a large gas carrier is $77,200; Miller, 2020). The Suez Canal obstruction in March 2021 highlighted the issues surrounding vessel passage through critical bottlenecks, causing an economic loss of 9 billion USD per day during the six-day obstruction (LaRocco, 2021). This intolerable congestion has disrupted the global supply chain, generated significant economic losses, and diminished the appeal of water transportation (Lave and DeSalvo, 1968; Laih and Sun, 2014; Laih et al., 2015; Rogers, 2018).

Improving the bottleneck's capacity is an effective way to mitigate the queues at waterway bottlenecks. However, this usually involves infrastructure expansions requiring large capital investment and long construction periods (Rusinov et al., 2021). Thus, waterway management authorities and shipping companies often prefer inexpensive and convenient congestion mitigation measures via vessel voyage rescheduling.

On the other hand, vessel voyage scheduling involves adjusting vessels' sailing speeds, which will affect the vessels' bunker cost. Note that the bunker cost constitutes 50–75% of the total operating cost of ships (Notteboom, 2006; Golias et al., 2009; Ronen, 2011; Dere and Deniz, 2019; Goicoechea and Abadie, 2021), and a vessel's bunker consumption increases

polynomially with the sailing speed (Wang et al., 2013). Thus, the vessel voyage scheduling optimization must consider both the schedule delay and bunker costs.

We next review the literature on vessel scheduling problems and bottleneck passage problems.

1.2 Literature review

1.2.1 Studies on bottleneck models

The vessel scheduling problem with bottleneck passage shares similarities with research on vehicle congestion at road traffic bottlenecks and congestion mitigation strategies. Numerous studies on road traffic bottleneck models aim to schedule vehicles passing through a bottleneck with limited capacity, minimizing total delay and schedule penalty costs (e.g., Xiao and Zhang, 2013; Small, 2015; Li et al., 2017; Yu et al., 2021; Cheng et al., 2022).

The first dynamic bottleneck model can be traced back to economist Vickrey (1969), featuring a deterministic model with one origin, one destination, and a single finite-capacity bottleneck. The cost function consists of travel time and schedule delay cost. Subsequent adaptations of Vickrey's model have emerged. Arnott et al. (1993) analyzed alternative pricing regimes (e.g., no toll, optimal uniform toll, optimal step toll, and optimal time-varying toll) and introduced elastic demand. Xiao and Zhang (2013) considered commuter time value in a single bottleneck model, deriving toll patterns, departure profiles, mode share, and user benefits during a morning commute. Chen et al. (2015) addressed step-tolled user equilibrium problems in bottleneck models with general user heterogeneity through semi-analytical and exact methods. The bottleneck model literature primarily stems from the realm of transportation economics, offering insights into congestion patterns and optimal pricing (Small, 2015). Dynamic bottleneck models are favored in road transportation research due to the endogeneity in vehicles' choices of travel schedules (de Palma and Lefèvre, 2019).

A body of research in this area focuses on the so-called "system optimal" solutions (Wardrop, 1952), where vehicle travel schedules are jointly optimized to minimize the total travel time and delay cost (Szeto and Lo, 2005; Zhang et al., 2017). Another set of studies

investigates feasible methods (e.g., toll schemes, tradable credits) to achieve or closely approximate the system optimal scheduling solution (Tian et al., 2013; Li et al., 2020). It is worth noting that a system optimal solution may not always be attainable due to practical reasons and constraints (the most significant being that each vehicle aims to maximize its own benefit rather than the collective benefit of the public). Nevertheless, examining the system optimum is valuable, as it provides a lower bound for the total system cost and serves as a benchmark to assess the effectiveness of management policies, such as pricing schemes.

A key result in road traffic bottleneck research is that vehicle queues at the bottleneck must be eliminated to achieve the system optimal solution. This can be understood by recognizing that if vehicles form a queue at a bottleneck, their arrival times at the bottleneck can be coordinated to prevent queueing without delaying their departure times from the bottleneck. Similarly, an analogous result can be derived for waterway bottlenecks: no vessel queue exists at the system optimum. Optimally coordinating vessel passage through the bottleneck not only eliminates queues but also reduces bunker costs, as vessels can maintain lower sailing speeds under coordination (Wang et al., 2013). Importantly, this holds true only when vessel travel schedules are jointly optimized.

However, road traffic bottleneck models are not directly applicable to our vessel scheduling problem for two reasons. First, these models primarily aim to minimize travelers' waiting times and schedule delay penalties, neglecting fuel cost considerations. As a result, they do not identify an optimal speed profile for minimizing fuel consumption, which is a critical aspect of vessel scheduling problems. Second, roadway traffic is typically modeled as a continuum owing to the high density of vehicles, whereas ships traversing a waterway are not treated as such due to their relatively sparse distribution in space and diverse operational characteristics.

1.2.2 Studies on vessel scheduling

The literature on vessel scheduling (e.g., Chen et al., 2021; Liu et al., 2022; Yang et al., 2023) has grown considerably over the past decades, including various problems characterized by distinct problem setups, application scopes, model formulations, and solution approaches

(Psaraftis, 2019). Comprehensive reviews of early studies in this realm can be found in Ronen (1983), Christiansen et al. (2004), Meng et al. (2014), and Chen et al. (2022).

Selected studies in the recent decade are summarized in Table 1. Most of them aimed to minimize the vessels' waiting time or cost, while others maximized the shipping profit (see column 2). Many studies assumed that the vessels sailed at a constant speed (column 3).

Table 1. Selected studies on ship scheduling problems.

Study	Objective	Varying speed	Bunker consumption	Bottleneck
Wang and Meng (2012)	Minimize cost	Yes	Yes	No
Hermans (2014)	Minimize wait time	No	No	Yes
Laih and Sun (2014)	Eliminate wait time	No	No	Yes
Meng et al. (2015)	Maximize profit	No	Yes	No
Passchyn et al. (2016)	Minimize wait time	No	No	Yes
Wen et al. (2016)	Maximize profit	Yes	Yes	No
Zhen et al. (2016)	Minimize cost	Yes	Yes	No
Lalla-Ruiz et al. (2018)	Minimize wait time	No	No	Yes
Tan et al. (2018)	Minimize bunker cost and trip time	Yes	Yes	Yes
Hill et al. (2019)	Minimize task completion time	No	No	Yes
Meisel and Fagerholt (2019)	Minimize transit time	Yes	No	Yes
Deng et al. (2021)	Minimize social cost	No	No	Yes
Schoeneich et al. (2023)	Assess safe maneuverability	No	No	Yes

More importantly, to our best knowledge, no work has jointly optimized multiple vessels' sailing speeds and bottleneck passage schedules to minimize the operating cost (see columns 4 and 5). The operating cost should include the bunker cost and the schedule delay penalty, both of which are functions of the vessel speed. Previous studies that considered the speed-dependent bunker consumption did not examine the effect of a waterway bottleneck where the vessel passages are dictated by a predefined capacity (Wang and Meng, 2012; Meng et al., 2015; Wen et al., 2016; Zhen et al., 2016). On the other hand, most works investigating vessel queueing at bottlenecks overlooked the relation between sailing speed and bunker cost (Hermans, 2014; Laih and Sun, 2014; Passchyn et al., 2016; Lalla-Ruiz et al., 2018; Hill et al., 2019; Deng et al., 2021). The only exception seems to be Tan et al. (2018), which developed a bi-objective

program to optimize ship sailing speeds and the schedule for visiting bottlenecks. Unfortunately, that work only focused on a single ship in the interest of deriving an analytical solution.

Regarding the solution approaches, scheduling problems are generally formulated as mathematical programs solved by various methods. These methods can be divided into exact solution approaches and heuristic approaches. The former includes analytical methods (Laih and Sun, 2014; Deng et al., 2021), branch-and-bound (Meng et al., 2015; Zhen et al., 2016; Hill et al., 2019), and Lagrange multiplier (Gu et al., 2012; Zhang et al., 2017). And examples of the latter include matheuristic methods (Meisel and Fagerholt, 2019), and greedy heuristics (Lalla-Ruiz et al., 2018). Many scheduling problem formulations are nonlinear, for which exact solutions are often intractable. Linearization techniques are therefore used.

For vessel scheduling problems, a key challenge lies in the nonlinear form of the bunker consumption function of speed. To address this challenge, Wang and Meng (2012) proposed an outer-approximation method, which used a combination of linear functions to approximate the nonlinear bunker consumption function. On the other hand, Wen et al. (2016) and Zhen et al. (2016) linearized their formulations by discretizing the ranges of speed and time, respectively. Theoretically, both types of methods can attain global optimality when certain parameters (i.e., the optimality tolerance level ε in the outer-approximation method and the discretization interval in the discretization methods) approach zero. However, their computational performances in solving real-sized problems were not adequately assessed and compared.

1.3 Overview of the paper

In light of the above gap in the literature, we formulate a novel model that optimizes multiple vessels' travel schedules for passing a common bottleneck. The objective is to minimize the total bunker cost and the schedule delay at their destinations. The model can be applied to any vessel scheduling problem involving a waterway bottleneck, regardless of whether the bottleneck is in a river or between oceans (e.g., the Suez and Panama Canals). After the infamous Suez Canal obstruction in 2021, issues related to vessel passages through critical bottlenecks have become increasingly important in recent years.

We concentrate on the system-optimal scheduling strategy, assuming the presence of a central operations manager responsible for coordinating the travel schedules and speed profiles of all vessels. The system-optimal solution can be achieved if all vessels belong to the same shipping company or are under the mandatory control of a bottleneck authority. For example, vessels passing through the Three Gorges Dam must report and register in advance, transferring control to the Three Gorges Navigation Authority during passage—this potentially allows the authority to act as a central operations manager. In situations where a central operations manager is not present, vessels operated by different companies will compete for bottleneck passages to minimize their individual costs, leading to a "user equilibrium" solution (Wardrop, 1952). In such cases, the system-optimal solution offers a lower bound on the total vessel cost and serves as a benchmark for evaluating the effectiveness of management policies, such as pricing schemes (e.g., Xiao and Zhang, 2013; Zhuge et al., 2021). Nevertheless, the examination of these management policies falls outside the scope of this paper and will be considered in future research.

We propose two alternative formulations to linearize the original nonlinear model. The first program used an improved outer-approximation method, originally proposed by Wang and Meng (2012), to approximate the nonlinear bunker cost function by a piecewise linear function. The second converts the nonlinear program to a binary integer program by discretizing the time. Their computational performances are evaluated and compared via extensive numerical experiments. Results show that the discrete-time model can produce better solutions within less runtime than the outer-approximation model, especially for large-scale problems. This finding reveals the numerical limitation of the outer-approximation method.

We use the Three Gorges Dam Lock as a case study to showcase the effectiveness of our model and the system-optimal scheduling strategy. Numerical results unveil how different vessels' optimal schedules and delays are affected by key operating parameters, including their delay penalty rates and fuel prices. The benefit of the system-optimal scheduling strategy is demonstrated via the comparison against two benchmark strategies. The first one assumes no coordination between vessels as each vessel individually determines its optimal sailing

schedule. The second assumes that a central operations manager determines the vessels' priority for bottleneck passage simply by their penalty rates.

Our main contributions are summarized as follows. First, our paper is the first to study the system-optimal scheduling strategy of vessels passing a common bottleneck, taking both bunker costs under varying speeds and schedule delay penalties into account. Second, we develop two linear approximation models for the problem, one using an improved outer-approximation method and the other by discretizing the time. By comparing the solution quality and computational efficiency of the two models, we show the limitation of the first linearization method. Lastly, our numerical analyses unveil the cost benefit of optimal schedule coordination compared to no coordination and naïve coordination strategies and how key operating factors affect optimal schedules and costs.

The rest of this paper is organized as follows. Section 2 defines the vessel scheduling problem involving a waterway bottleneck and presents the model formulations. Section 3 compares the two alternative programs' solution quality and computational efficiency. Numerical results of the TGD case study are presented in Section 4, including the comparison against two benchmark scheduling strategies. Key findings and their implications on theory and practice are discussed in Section 5. Conclusions and future research directions are summarized in Section 6.

2. Models

Section 2.1 introduces the problem definition and key assumptions. Section 2.2 presents the problem formulation. Sections 2.3 and 2.4 furnish the outer-approximation and discrete-time formulations, respectively. New notations are defined at their first appearance and are summarized following each model formulation.

2.1 Problem setup and assumptions

Consider a set of vessels, denoted by V, that pass a common bottleneck in a waterway network, e.g., a dam or canal. The vessel fleet may comprise a combination of cargo vessels, such as container ships, dry bulk carriers, and tankers, as well as other types of vessels,

including pleasure crafts. Each vessel $v \in V$ departs its distinct origin port of call at time T_v^0 and is expected to arrive at its destination port by T_v. The travel distances from vessel v's origin port to the bottleneck (the first leg of its voyage) and from the bottleneck to its destination port (the second leg) are denoted by L_{1v} and L_{2v} (nautical miles), respectively. We assume that each vessel spends a constant transit time, ω (h), on traversing the bottleneck and that a minimum headway between two consecutive vessel passages through the bottleneck, H (h), is required to ensure safety. Fig. 1 illustrates a typical process of vessels passing a waterway bottleneck. A vessel that cannot pass the bottleneck immediately upon arrival will join a queue. A vessel that arrives at its destination port later than the expected arrival time will incur a penalty.

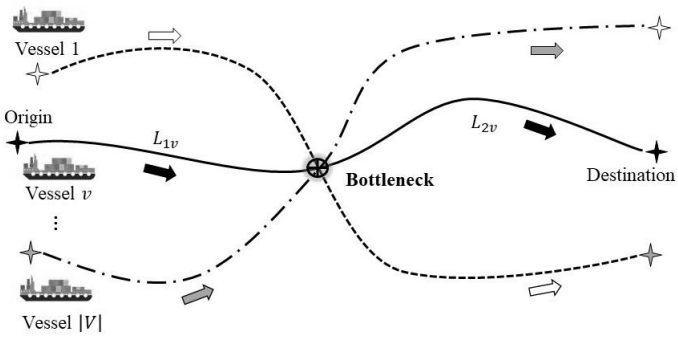

Fig. 1. A typical process of vessels passing a waterway bottleneck.

To derive the system optimal scheduling solution, we assume that a central operations manager seeks to minimize the total bunker consumption and late arrival penalty for all the vessels. The bunker consumption rate of vessel v (ton/n mile) depends on its sailing speed s (knot). In this paper, we use the bunker consumption rate function proposed by Wang and Meng (2012):

$$f_v(s) = a_v \cdot s^{b_v}, v \in V \quad (1)$$

where $f_v(s)$ denotes the bunker consumption per nautical mile of vessel $v \in V$; and $a_v > 0$ and $b_v > 1$ are constant coefficients.[1] Vessel v's tardiness penalty, P_v ($), is assumed to be

[1] Note that Equation (1) can be replaced with other bunker consumption functions. The methodology proposed in this paper can still be used as long as the function is convex (the readers may refer to, e.g., von Westarp, 2020, and Du et al., 2011, for alternative bunker consumption relations).

a linear function of its delay; i.e., $P_v(y_v) = \beta_v \cdot \max\{0, y_v - T_v\}$, where β_v (\$/h) denotes the penalty per hour of delay, and y_v the actual arrival time of v at its destination port.

We derive the following two propositions from Equation (1):

Proposition 1. For a fixed travel distance, a vessel's bunker consumption increases with its speed.

Proposition 2. A vessel will travel at a constant speed to minimize the bunker consumption if the travel distance and time are both fixed.

Proposition 1 follows directly from the monotonicity of Equation (1). Proposition 2 can be proved by using the strict convexity of the bunker consumption per hour, i.e., $f_v(s) \cdot s = a_v s^{b_v+1}$. Suppose vessel v's travel distance and time are L and t, respectively. It travels at speed s_1 for δt hours and at $s_2 \neq s_1$ for $(1-\delta)t$ hours $(0 < \delta < 1)$ so that $s_1\delta t + s_2(1-\delta)t = L$. The total bunker consumption is $\big(f_v(s_1)s_1\delta + f_v(s_2)s_2(1-\delta)\big)t$. If the vessel travels at its average speed, $s_1\delta + s_2(1-\delta)$, it will cover the same distance L in the same duration t. However, it will use less fuel because the strict convexity of $f_v(s) \cdot s$ renders $f_v\big(s_1\delta + s_2(1-\delta)\big) \cdot \big(s_1\delta + s_2(1-\delta)\big)t < f_v(s_1)s_1\delta t + f_v(s_2)s_2(1-\delta)t$.

Proposition 1 yields the following two corollaries:

Corollary 1. It is never optimal for a vessel to arrive earlier than its expected arrival time.

Corollary 2. Under the system-optimal scheduling strategy, it is never optimal for vessels to form a queue at the bottleneck.

Corollary 1 is true because if a vessel arrives earlier than its expected arrival time, it can always lower its speed to reduce the bunker consumption while still arriving on time. Corollary 2 holds because the central operations manager can always coordinate the vessels to sail more slowly to eliminate queues at the bottleneck without further delaying any vessel's passage. Then the bunker costs would be reduced without increasing the schedule delay penalties.

In addition, Proposition 2 indicates that each vessel will travel at constant speeds on the first and second legs of its voyage. Thus, we denote x_v the arrival time of vessel $v \in V$ at the

bottleneck. Following the above corollaries, vessel v's cruise speeds on the first and second legs are $\frac{L_{1v}}{x_v - T_v^0}$ and $\frac{L_{2v}}{y_v - x_v - \omega}$, respectively.

The problem is therefore equivalent to finding the optimal x_v and y_v $(v \in V)$ for minimizing the total bunker consumption and penalty costs. We next formulate a nonlinear program for the problem.

2.2 Problem formulation

The system-optimal formulation for the vessel scheduling problem with bottleneck passage is presented as follows:

[M1]

$$\min \sum_{v \in V} \left\{ \alpha \left[L_{1v} a_v \left(\frac{L_{1v}}{x_v - T_v^0} \right)^{b_v} + L_{2v} a_v \left(\frac{L_{2v}}{y_v - x_v - \omega} \right)^{b_v} \right] + \beta_v \cdot \max\{0, y_v - T_v\} \right\} \quad (2a)$$

subject to

$$x_v \geq T_v^0 + \frac{L_{1v}}{s_v^{\max}}, \forall v \in V \quad (2b)$$

$$y_v \geq x_v + \omega + \frac{L_{2v}}{s_v^{\max}}, \forall v \in V \quad (2c)$$

$$|x_i - x_j| \geq H, \forall i, j \in V, i \neq j. \quad (2d)$$

The notations are explained as follows:

v, i, j	vessel indices;
$x_v,\ y_v$	(h), arrival times of vessel v at the bottleneck and its destination port;
$L_{1v},\ L_{2v}$	(n mile), distances from vessel v's origin port to the bottleneck and from the bottleneck to its destination port;
T_v^0	(h), vessel v's departure time from its origin port;
T_v	(h), vessel v's expected arrival time at its destination port;
β_v	($/h), tardiness penalty per hour of vessel v;
$a_v,\ b_v$	coefficients of the bunker consumption function, $a_v > 0,\ b_v > 1$;
$s_v^{\max}$	(knot), the maximum sailing speed of vessel v;
ω	(h), transit time for a vessel to pass through the bottleneck;

H (h), the minimum headway between the passages of two consecutive vessels through the bottleneck;

α ($/ton), bunker fuel price.

In objective function (2a), the first term in the braces is the bunker consumption cost of vessel $v \in V$, where α denotes the bunker fuel price ($/ton); and the second term is the vessel's tardiness penalty. Constraints (2b) and (2c) guarantee that a vessel's sailing speed never exceeds a maximum speed, $s_v^{\max}$ (knot). Constraints (2d) stipulate the minimum headway between the passages of any two vessels through the bottleneck.

[M1] is a nonlinear program with a nonlinear objective (2a) and nonlinear constraints (2d). Constraints (2d) can be linearized using some techniques like the Big-M method. The objective function, especially the nonlinear bunker cost function, can be replaced by a piece-wise linear approximation (like the outer-approximation method in Wang and Meng, 2012). Additionally, since all decision variables are time variables, discretizing [M1] in time can also transform it into a mixed integer linear program. These two approaches (outer-approximation and discretization) are commonly found in the literature. In order to evaluate their performance and identify the more effective method under different operating conditions, we proceed to linearize [M1] using the two approaches described in the subsequent subsections.[2]

2.3 Linearization via the outer-approximation method

Constraints (2d) can be linearized as follows using the Big-M method:

$$x_i - x_j \geq H + M(z_{ij} - 1), \forall i, j \in V, i \neq j \quad (3a)$$

$$x_i - x_j \leq -H + M z_{ij}, \forall i, j \in V, i \neq j \quad (3b)$$

where M is a sufficiently large number, and z_{ij}'s $(i, j \in V)$ are binary variables. The $z_{ij} = 1$ if vessel i arrives at the bottleneck after vessel j, and $= 0$ otherwise. A candidate value of M will be provided momentarily.

[2] While other methods may exist, their applications are rare and usually have special requirements for the program being solved. As of now, we are not aware of any other methods applicable to our vessel scheduling problem involving a bottleneck.

Next, we linearize the objective function (2a). First, the penalty term can be linearized by introducing a nonnegative auxiliary variable p_v ($v \in V$) that represents vessel v's delay. The penalty term in (2a) is then replaced with $\beta_v p_v$. In addition, the following constraints are added to the formulation:

$$p_v \geq 0, \forall v \in V \tag{4a}$$

$$p_v \geq y_v - T_v, \forall v \in V. \tag{4b}$$

Finally, we linearize the bunker fuel cost term in (2a) via the outer-approximation method. To this end, we first replace decision variables x_v and y_v with vessel v's travel times in the two segments, denoted by λ_v and μ_v ($v \in V$), respectively, i.e.,

$$\lambda_v = x_v - T_v^0, \forall v \in V \tag{5a}$$

$$\mu_v = y_v - x_v - \omega, \forall v \in V. \tag{5b}$$

Thus, constraints (2b–c), (3a–b), and (4b) are rewritten as:

$$\lambda_v \geq \lambda_v^{\min} \equiv \frac{L_{1v}}{s_v^{\max}}, \forall v \in V \tag{6a}$$

$$\mu_v \geq \mu_v^{\min} \equiv \frac{L_{2v}}{s_v^{\max}}, \forall v \in V \tag{6b}$$

$$\lambda_i - \lambda_j \geq H - T_i^0 + T_j^0 + M(z_{ij} - 1), \forall i, j \in V, i \neq j \tag{6c}$$

$$\lambda_i - \lambda_j \leq -H - T_i^0 + T_j^0 + M z_{ij}, \forall i, j \in V, i \neq j \tag{6d}$$

$$p_v \geq T_v^0 + \lambda_v + \omega + \mu_v - T_v, \forall v \in V. \tag{6e}$$

The bunker consumption in (2a) is now rewritten as $L_{1v} a_v \left(\frac{L_{1v}}{\lambda_v}\right)^{b_v} + L_{2v} a_v \left(\frac{L_{2v}}{\mu_v}\right)^{b_v}$. To linearize this term, we define $Q_{1v}(\lambda_v)$ and $Q_{2v}(\mu_v)$ as follows:

$$Q_{1v}(\lambda_v) = a_v \left(\frac{L_{1v}}{\lambda_v}\right)^{b_v}, \forall v \in V \tag{7a}$$

$$Q_{2v}(\mu_v) = a_v \left(\frac{L_{2v}}{\mu_v}\right)^{b_v}, \forall v \in V. \tag{7b}$$

Since $b_v > 1$, $Q_{1v}(\lambda_v)$ and $Q_{2v}(\mu_v)$ are convex functions. They are approximated by piecewise-linear, lower-bound functions denoted by $\overline{Q}_{1v}(\lambda_v)$ and $\overline{Q}_{2v}(\mu_v)$:

$$\overline{Q}_{1v}(\lambda_v) = \max\{0, \theta_{1vk}\lambda_v + \gamma_{1vk}, \forall k = 1,2,\cdots,K_{1v}\}, v \in V \tag{8a}$$

$$\overline{Q}_{2v}(\mu_v) = \max\{0, \theta_{2vk}\mu_v + \gamma_{2vk}, \forall k = 1,2,\cdots,K_{2v}\}, v \in V \tag{8b}$$

where θ_{1vk}, γ_{1vk}, θ_{2vk}, and γ_{2vk} are coefficients of the linear segments used to construct the approximate functions; and K_{1v} and K_{2v} are the numbers of linear segments. The two functions are constructed to ensure the approximation error of the total bunker cost never exceeds a predefined bound ε (\$), i.e., $\alpha \sum_{v\in V} \left|\left(L_{1v}\overline{Q}_{1v}(\lambda_v) + L_{2v}\overline{Q}_{2v}(\mu_v)\right) - \left(L_{1v}Q_{1v}(\lambda_v) + L_{2v}Q_{2v}(\mu_v)\right)\right| \leq \varepsilon$. The concept is straightforward: create a series of linear segments that are tangent to the nonlinear function ($Q_{1v}(\lambda_v)$ or $Q_{2v}(\mu_v)$) and constrained by an error bound derived from ε, ensuring that the error in the total bunker cost remains within ε. Appendix A provides a detailed description of the algorithm for constructing $\overline{Q}_{1v}(\lambda_v)$ and $\overline{Q}_{2v}(\mu_v)$, including the determination of coefficients θ_{1vk}, γ_{1vk} $(v \in V, k = 1,2,\dots,K_{1v})$, θ_{2vk}, and γ_{2vk} $(v \in V, k = 1,2,\dots,K_{2v})$. The algorithm is designed to use as few linear segments as possible while maintaining the desired level of accuracy.

Built upon the above approximations, we introduce new decision variables q_{1v} and q_{2v} denoting the bunker consumption rates of vessel v's two trip legs ($v \in V$). Then [M1] is approximated by the following mixed-integer linear program:

[M2]

$$\min \sum_{v\in V}\{\alpha[L_{1v}q_{1v} + L_{2v}q_{2v}] + \beta_v p_v\} \quad (9a)$$

subject to

Constraints (4a), (6a–e), and

$$q_{1v} \geq \theta_{1vk}\lambda_v + \gamma_{1vk}, q_{1v} \geq 0, \forall k = 1,2,\cdots,K_{1v}, \forall v \in V \quad (9b)$$

$$q_{2v} \geq \theta_{2vk}\mu_v + \gamma_{2vk}, q_{2v} \geq 0, \forall k = 1,2,\cdots,K_{2v}, \forall v \in V. \quad (9c)$$

The new notations are:

q_{1v}, q_{2v} (ton/n mile), bunker consumption rates of vessel v on its first and second sailing legs;

λ_v, μ_v (h), vessel v's travel times on its first and second sailing legs;

p_v (h), vessel v's delay at its destination port;

θ_{1vk}, γ_{1vk} slopes and intercepts of the linear segments used to construct the outer approximation $\overline{Q}_{1v}(\lambda_v)$, $k \in \{1,2,\dots,K_{1v}\}$;

θ_{2vk}, γ_{2vk} slopes and intercepts of the linear segments used to construct $\overline{Q}_{2v}(\mu_v)$, $k \in \{1,2,\dots,K_{2v}\}$;

K_{1v}, K_{2v} number of linear segments used to construct $\overline{Q}_{1v}(\lambda_v)$ and $\overline{Q}_{2v}(\mu_v)$.

Program [M2] can be solved via commercial solvers like CPLEX. However, the computation cost rises rapidly with the number of constraints dictated by K_{1v} and K_{2v} ($v \in V$). To improve the solution efficiency, we improve the original outer-approximation method by developing tight bounds for the optimal λ_v and μ_v. These bounds can effectively diminish the search ranges for the optimal λ_v and μ_v, and thus reduce the numbers of linear segments used in constraints (8a–b).

Specifically, the upper bounds of λ_v and μ_v, denoted by $\lambda_v^{\max}$ and $\mu_v^{\max}$ respectively, are presented as follows:

$$\lambda_v^{\max} = \max\left\{\max\left\{T_v - T_v^0 - \omega - \frac{L_{2v}}{s_v^{\max}},\ L_{1v}\left(\frac{\alpha a_v b_v}{\beta_v}\right)^{\frac{1}{b_v+1}}\right\} + 2(|V|-1)H, \frac{L_{1v}}{s_v^{\max}}\right\}, \forall v \in V \quad (10a)$$

$$\mu_v^{\max} = \max\left\{T_v - T_v^0 - \omega - \frac{L_{1v}}{s_v^{\max}}, L_{2v}\left(\frac{\alpha a_v b_v}{\beta_v}\right)^{\frac{1}{b_v+1}},\ \frac{L_{2v}}{s_v^{\max}}\right\}, \forall v \in V. \quad (10b)$$

Proofs of the above upper bounds are relegated to Appendix B. In addition, the lower bounds of the optimal λ_v and μ_v are given by Equations (6a–b).

Finally, by scrutinizing (6c – d), we find that the following value of M is sufficiently large to use:

$$M = H + \max_{v \in V} T_v^0 - \min_{v \in V} T_v^0 + \max_{v \in V} \lambda_v^{\max} - \min_{v \in V} \lambda_v^{\min}. \quad (11)$$

Any value greater than (11) can also be used. However, using a larger M would increase the solution time of [M2].

2.4 A discrete-time model

We now discretize the time variables in [M1] using a unit time interval denoted by Δt. Time discretization essentially discretizes the range of speeds each vessel can take in its two

sailing legs. Thus, the bunker consumption rate for each discrete speed value can be calculated in advance, eliminating the nonlinearity issue. Note that the travel time bounds developed in Section 2.3 also allow us to use as few time intervals as possible, thus improving the computational efficiency of the discrete-time model.

Specifically, define $\tau \in Z_+$ as the integer time coordinate, where Z_+ represents the set of all positive integers. Denote Ψ_{1v} the set of possible arrival times of vessel $v \in V$ at the bottleneck, and Ψ_{2v} the set of possible travel times of vessel v for the second sailing leg. They are given by:

$$\Psi_{1v} = \{\tau | \tau \in Z_+, \frac{1}{\Delta t}(T_v^0 + \lambda_v^{\min}) \le \tau \le \frac{1}{\Delta t}(T_v^0 + \lambda_v^{\max})\}, \forall v \in V \quad (12a)$$

$$\Psi_{2v} = \{\tau | \tau \in Z_+, \frac{1}{\Delta t}(\omega + \mu_v^{\min}) \le \tau \le \frac{1}{\Delta t}(\omega + \mu_v^{\max})\}, \forall v \in V \quad (12b)$$

where $\lambda_v^{\min}$, $\lambda_v^{\max}$, $\mu_v^{\min}$, and $\mu_v^{\max}$ can be found in Equations (6a–b) and (10a–b).

Define two batches of binary decision variables, $x_{\tau v}$ and $\xi_{\tau v}$, to substitute for x_v and y_v. Specifically, $x_{\tau v} = 1$ if and only if $x_v = \Delta t \cdot \tau$, and $\xi_{\tau v} = 1$ if and only if $y_v - x_v = \Delta t \cdot \tau$. We have the following constraints for the discrete-time model:

$$\sum_{\tau \in \Psi_{1v}} x_{\tau v} = 1, \forall v \in V \quad (13a)$$

$$\sum_{\tau \in \Psi_{2v}} \xi_{\tau v} = 1, \forall v \in V \quad (13b)$$

$$x_{\tau v} \in \{0,1\}, \forall \tau \in \Psi_{1v}, \forall v \in V \quad (13c)$$

$$\xi_{\tau v} \in \{0,1\}, \forall \tau \in \Psi_{2v}, \forall v \in V. \quad (13d)$$

Constraints (13a) and (13b) will replace (2b) and (2c) in the original program [M1].

Further, denote $\tau_1^{\min} = \min\{\tau \in \cup_{v \in V} \Psi_{1v}\}$ and $\tau_1^{\max} = \max\{\tau \in \cup_{v \in V} \Psi_{1v}\}$ the minimum and maximum arrival times of all vessels at the bottleneck, and $h' = H/\Delta t$. We select the Δt such that h' is an integer. Then constraints (2d) in [M1] can be replaced with the following one, which stipulates that at most one vessel will arrive at the bottleneck during any h' consecutive time intervals:

$$\sum_{v \in V} \sum_{\tau \in \Psi_{1v} \cap \{i, \dots, i+h'-1\}} x_{\tau v} \le 1, \quad i = \tau_1^{min}, \tau_1^{min} + 1, \cdots, \tau_1^{max} - h' + 1. \quad (14)$$

In the discrete-time model, the penalty term in the objective (2a), $\beta_v \cdot \max\{0, y_v - T_v\}$, is also linearized as described in Section 2.3. The associated constraints (4a) are retained, while constraints (4b) are replaced with:

$$p_v \geq \sum_{\tau \in \Psi_{1v}} \Delta t \cdot \tau \cdot x_{\tau v} + \sum_{\tau \in \Psi_{2v}} \Delta t \cdot \tau \cdot \xi_{\tau v} - T_v, \forall v \in V. \quad (15)$$

This is because $y_v = \sum_{\tau \in \Psi_{1v}} \Delta t \cdot \tau \cdot x_{\tau v} + \sum_{\tau \in \Psi_{2v}} \Delta t \cdot \tau \cdot \xi_{\tau v}$, and $x_v = \sum_{\tau \in \Psi_{1v}} \Delta t \cdot \tau \cdot x_{\tau v}, \forall v \in V$.

Finally, the bunker fuel cost term in (2a), $\alpha \left[L_{1v} a_v \left(\frac{L_{1v}}{x_v - T_v^0} \right)^{b_v} + L_{2v} a_v \left(\frac{L_{2v}}{y_v - x_v - \omega} \right)^{b_v} \right]$, is rewritten as $\alpha [L_{1v} Q_{1v} + L_{2v} Q_{2v}]$, where Q_{1v} and Q_{2v} are expressed as functions of $x_{\tau v}$ and $\xi_{\tau v}$:

$$Q_{1v} = \sum_{\tau \in \Psi_{1v}} a_v \left(\frac{L_{1v}}{\Delta t \cdot \tau - T_v^0} \right)^{b_v} x_{\tau v}, \forall v \in V \quad (16a)$$

$$Q_{2v} = \sum_{\tau \in \Psi_{2v}} a_v \left(\frac{L_{2v}}{\Delta t \cdot \tau - \omega} \right)^{b_v} \xi_{\tau v}, \forall v \in V. \quad (16b)$$

In summary, program [M1] can be converted to the following binary integer program:

[M3]

$$\min \sum_{v \in V} \left\{ \alpha \left[L_{1v} \sum_{\tau \in \Psi_{1v}} a_v \left(\frac{L_{1v}}{\Delta t \cdot \tau - T_v^0} \right)^{b_v} x_{\tau v} + L_{2v} \sum_{\tau \in \Psi_{2v}} a_v \left(\frac{L_{2v}}{\Delta t \cdot \tau - \omega} \right)^{b_v} \xi_{\tau v} \right] + \beta_v p_v \right\} \quad (17)$$

subject to

Constraints (4a), (13a–d), (14) and (15).

The new notations introduced into this formulation are summarized as follows:

τ	time coordinate in the discrete-time model;
Δt	(h), unit time interval in the discrete-time model;
Ψ_{1v}	set of all the possible arrival times of vessel v at the bottleneck in the discrete-time model;
Ψ_{2v}	set of all the possible travel times of vessel v on its second sailing leg in the discrete-time model;
$x_{\tau v}$	binary variable that equals 1 if vessel v arrives at the bottleneck at τ, and 0 otherwise;

$\xi_{\tau v}$ binary variable that equals 1 if vessel v's travel time from entering the bottleneck to arriving at its destination port is τ, and 0 otherwise;

$Q_{1v}(\lambda_v)$ (ton/n mile), bunker consumption rate of vessel v for travel time λ_v on the first sailing leg;

$Q_{2v}(\mu_v)$ (ton/n mile), bunker consumption rate of vessel v for travel time μ_v on the second sailing leg;

h' number of time intervals representing the minimum headway between the passages of two consecutive vessels through the bottleneck in the discrete-time model.

[M3] can also be solved by CPLEX.

3. Solution quality and computational efficiency

This section looks into the solution quality and computational efficiency of models [M2] and [M3]. We first consider 100 randomly generated numerical instances with 12 vessels. The parameters of each instance, i.e., L_{1v}, L_{2v}, T_v^0, T_v, β_v, $s_v^{\max}$, a_v and b_v for $v \in \{1,2,\dots,12\}$, are generated from the following distributions: $L_{1v}, L_{2v} \sim U[31, 360]$ n miles, $T_v^0 \sim U[0.1, 30]$ hours, $T_v \sim U[30, 60]$ hours, $\beta_v \sim U[1000, 6000]$ \$/h, $s_v^{\max} \sim U[18, 23]$ knot, $a_v \sim U[4, 5] \times 10^{-4}$, $b_v \sim U[1.8, 2.2]$, where $U[c_1, c_2]$ denotes a uniform distribution with support from c_1 to c_2. Normally, the maximum sailing speed of cargo vessel varies around 20 knots (Karsten et al., 2018; Zheng et al., 2021). The coefficient b_v of bunker consumption rate function is around 2, while the coefficient a_v mainly depends on the vessel's type, size, and engine (Wang and Meng, 2012; Andersson et al., 2015; von Westarp, 2020; Zheng et al., 2021). Likewise, the penalty rate β_v varies based on factors such as the vessel's type, size and crew, as well as the cargo type and value. The bunker fuel price α, the vessel transit time through the bottleneck ω, and the minimum headway H are set to 500 \$/ton (Ship and Bunker, 2023), 3 hours, and 1 hour, respectively (Sina News, 2020). In addition, we specify seven values of the error bound ε in [M2], i.e., $\varepsilon \in \{625, 312.5, 156.3, 78.1, 39.1, 19.5, 9.8\}$ \$, and seven values

of the time interval Δt in [M3]: $\Delta t \in \left\{1, \frac{1}{2}, \frac{1}{4}, \frac{1}{8}, \frac{1}{16}, \frac{1}{32}, \frac{1}{64}\right\}$ hour. Note that both ε and Δt decrease at a rate of 0.5 in the above sequences. Models [M2] and [M3] are solved by CPLEX-12.8 running on a 4.7 GHz Octa-Core PC with 32 GB of RAM.

Solutions obtained from the two approximate models [M2] and [M3] are plugged into (2a) to calculate the true objective values. Thus, the results are upper bounds of the optimal solution. For simplicity, we calculate the averages of each model's objective values and runtimes across the 100 numerical instances. The average values of [M2] are plotted against ε in Fig. 2a, and those of [M3] are plotted against Δt in Fig. 2b. Note that the horizontal axis is set to the logarithmic scale in each figure.

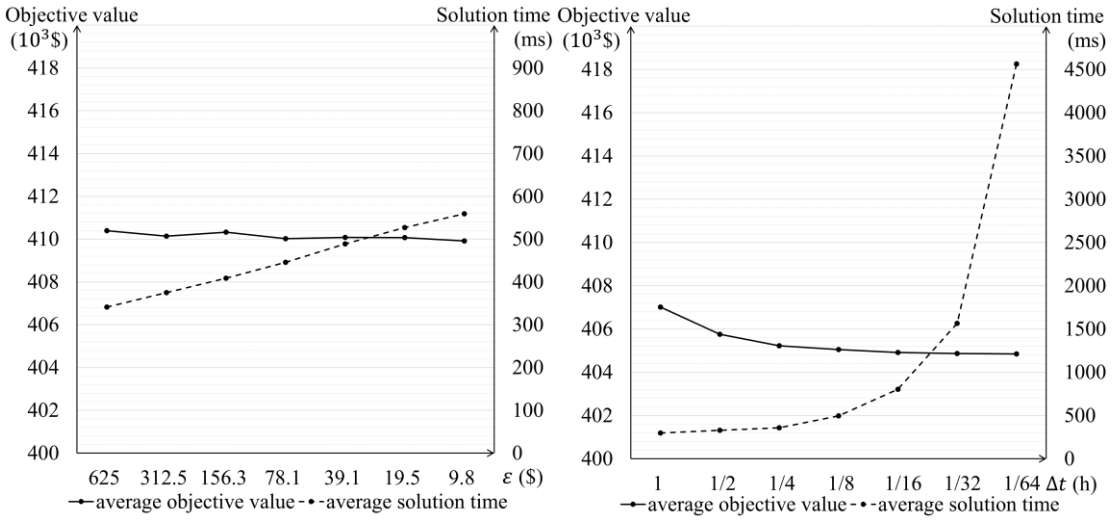

(a) Outer-approximation model [M2] (b) Discrete-time model [M3]

Fig. 2. Objective values and solution times of the two models.

Both figures show that the average objective value (the solid curve) decreases as ε or Δt diminishes. However, the two solid curves exhibit different patterns. The average objective value calculated from [M3] quickly converges to 4.05×10^5 \$ as $\Delta t \leq \frac{1}{8}$ hour, manifesting that the solution to [M3] converges to the exact solution of [M1] as Δt approaches zero. On the other hand, the objective value obtained from [M2] oscillates around 4.10×10^5 \$ when $\varepsilon \leq 312.5$ \$. This reveals that the solution of [M2] has a larger error than that of [M3]. (Recall that the curves show the true objective values calculated by the original objective function (2a), and they are upper bounds of the exact solution of [M1].) Using the convergent objective value of [M3] as the benchmark, the solution to [M2] exhibits an error of at least 1.2%. More

importantly, further numerical analyses showed that this error did not diminish when ε approaches zero, meaning *the predefined "error bound" ε cannot be guaranteed*. A potential cause for the error exceeding its designated bound lies in the piecewise linear approximation of nonlinear functions $Q_{1v}(\lambda_v)$ and $Q_{2v}(\mu_v)$. Specifically, numerical error arises when calculating the lines and points of tangency in the piecewise linear approximation of [M2] (see Algorithm 1 in Appendix A). Regrettably, this error tends to fluctuate as ε approaches zero since the start point of each tangent line segment becomes closer to the original curve. Please refer to the end of Appendix A for a more detailed explanation.

On the other hand, the average runtime increases as ε or Δt diminishes; see the dashed curves in Fig. 2a and b. This observation is expected. The runtime in Fig. 2b increases rapidly since the number of constraints in [M3] grows linearly with the number of time intervals; see Equation (14). Nevertheless, Fig. 2b shows that the solution quality is good enough for $\Delta t \leq \frac{1}{8}$ hour. The benefit of further reducing Δt is negligible.

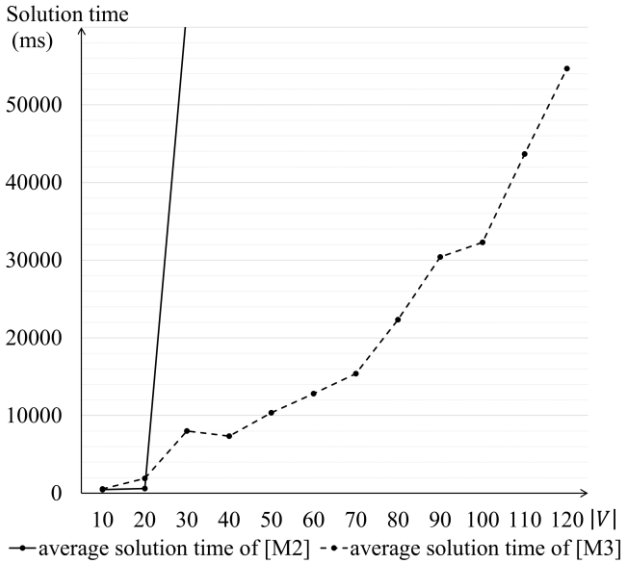

Fig. 3. Comparison of solution times of [M2] and [M3] for $|V| \in [10, 120]$.

A more important question is how the two models perform when solving larger-scale instances. Fig. 3 plots the average runtimes of 100 randomly selected instances for [M2] and [M3] when the number of vessels $|V|$ varies from 10 to 120. For each value of $|V|$, the same 100 instances are solved by both models. The ε and Δt are set to 1,000 $ and 0.1 hour, respectively. These values are selected in favor of [M2] in terms of the runtime; see Fig. 2a and

b. Other values of ε and Δt yield similar results as Fig. 3. The other parameter values are the same as for Fig. 2a and b. Fig. 3 shows that the runtime of [M2] soars when $|V| > 20$, making [M2] unacceptably slow for large-scale vessel scheduling problems. The reason is simple. Note that the number of piecewise linear constraints (9b) and (9c) in [M2] increases rapidly with $|V|$. Furthermore, the number of constraints (6c) and (6d) increases quadratically with $|V|$. These problems do not exist for [M3].

In summary, [M3] appears to be a better choice than [M2] in terms of both solution quality and computational efficiency, especially for large-scale problems.

4. Numerical case study

The background and parameter values of a real-life case study are introduced in Section 4.1. Section 4.2 examines the optimal vessel schedules and the associated delays obtained from the two models. The benefit of the optimal coordination of vessel passages at the bottleneck is investigated in Section 4.3.

4.1 Case description

In this paper, we choose the vessels traversing the Three Gorges Dam Lock as the subject of our case study. It is important to note that the models and solution methods presented above can be applied to any bottlenecks encountered in both seaborne and river-borne transport.

The Three Gorges Dam on the Yangtze River is one of the busiest waterway bottlenecks in the world (Pomfret, 2019). We consider a simple case with 12 vessels passing through the TGD lock. The maximum sailing speeds and bunker consumption parameters of the 12 vessels are again randomly generated according to the same value ranges specified in Section 3 (see the justification of these value ranges in Section 3). They are summarized in Table 2. Columns 2–5 of Table 3 show the 12 vessels' origin and destination ports and their distances from the TGD. These origin and destination ports are randomly selected from major ports along the waterway segment between Hankou Port and Chongqing Port, which is a typical stretch containing the Three Gorges Dam. The locations of these ports and the TGD on the Yangtze River are illustrated in Fig. 4. Columns 6–11 of Table 3 show their departure times, expected

arrival times, and penalty rates for two scenarios. These parameter values are selected in a way that the vessels' sailing time windows ($T_v - T_v^0$) in Scenario 1 are generally tighter than in Scenario 2, while the penalty rates in Scenario 2 are higher. By comparing these two scenarios, we can examine how the vessels' travel time windows and penalty rates β_v affect the optimal vessel schedules and actual arrival times at the destinations. The vessel transit time ω and the minimum headway H are set to 3 hours and 1 hour, respectively (Sina News, 2020). According to Ship and Bunker (2023), the current bunker fuel price is approximately \$550 per ton, and it has fluctuated between \$200 and \$1000 per ton over the past three years. Consequently, we employ three representative prices—\$200, \$500, and \$800 per ton—in the numerical case study to account for the variations in the fuel market. Comparing the solutions under different fuel prices can unveil how the fuel price affects the optimal vessel schedules and delays. For the outer-approximation model [M2], the error bound ε is set to 1,000 \$. For the discrete-time model [M3], the unit time interval Δt is set to 0.1 hour.

Table 2. Maximum sailing speeds and bunker consumption parameters.

Vessel	1	2	3	4	5	6	7	8	9	10	11	12
$s_v^{\max}$ (knot)	19	20	19	18	21	23	19	18	22	20	21	19
a_v (10^{-4})	4.2	4.0	4.3	4.2	4.3	4.4	4.5	4.1	4.2	4.3	4.1	4.3
b_v	1.95	2.10	1.98	2.05	2.02	1.96	1.89	1.96	2.04	1.97	2.10	2.11

Fig. 4. Locations of the origin and destination ports and the TGD along the Yangtze River.

Table 3. Vessel route parameters, departure and expected arrival times, and penalty rates.

Vessel	Origin	Destination	L_{1v} (n mile)	L_{2v} (n mile)	Scenario 1			Scenario 2		
					T_v^0 (h)	T_v (h)	β_v (\$/h)	T_v^0 (h)	T_v (h)	β_v (\$/h)
1	Zhicheng	Badong	51.84	31.86	23.8	32.5	1000	23.3	30.2	4000
2	Zhicheng	Wanxian	51.84	145.79	23.3	41.2	1200	19.7	30.2	4200
3	Shashi	Fuling	101.51	257.56	19.7	47.8	1500	19.7	41.6	4500
4	Shashi	Chongqing	101.51	322.35	23.7	49.8	1900	23.3	41.6	4900
5	Shashi	Badong	101.51	31.86	21.7	31.5	2100	8.2	52.8	4100
6	Chenglingji	Wanxian	234.88	145.79	11.2	40.2	2400	1.3	59.2	4400
7	Chenglingji	Fuling	234.88	257.56	12.5	41.1	3900	1.3	41.6	4900
8	Chenglingji	Chongqing	234.88	322.35	13.5	46.1	5000	10.2	51.2	5000
9	Honghu	Badong	262.96	31.86	10.6	24.7	5200	10.2	59.2	5200
10	Honghu	Wanxian	262.96	145.79	10.1	31.2	5400	8.2	59.2	5400
11	Hankou	Fuling	359.61	257.56	2.3	40.8	5700	1.3	52.8	5700
12	Hankou	Wanxian	359.61	145.79	3.3	36.2	5000	1.3	59.2	5000

4.2 Optimal vessel scheduling solutions

Fig. 5a and b plot the optimal total cost, the tardiness penalty, and the bunker cost against the bunker price α for the two scenarios, respectively. Results of [M2] and [M3] are plotted as the solid and dashed curves, respectively. Note that the optimal cost values calculated by the two models are very close to each other in most cases. An exception occurs when $\alpha = 800$ \$/ton under Scenario 1, where the gaps in the bunker cost and the tardiness penalty between the two models are 7% and 46%, respectively. These large gaps are possibly due to the inaccuracy of the approximation in [M2].

As expected, the total cost increases rapidly as α grows in each scenario. The increase is mainly due to the surge in the bunker cost. The tardiness penalty also increases since vessels will reduce their speeds to save the bunker at a higher price, although that would result in larger schedule delays. The difference between the two scenarios is also evident. In Scenario 1, the tardiness penalty increases by 78% (using the more accurate result of [M3]) when α rises from 200 to 800 \$/ton since more vessels choose to bear greater delays with the lower tardiness penalty rates. However, for the same case in Scenario 2, the tardiness penalty only increases by 13% due to the higher penalty rates.

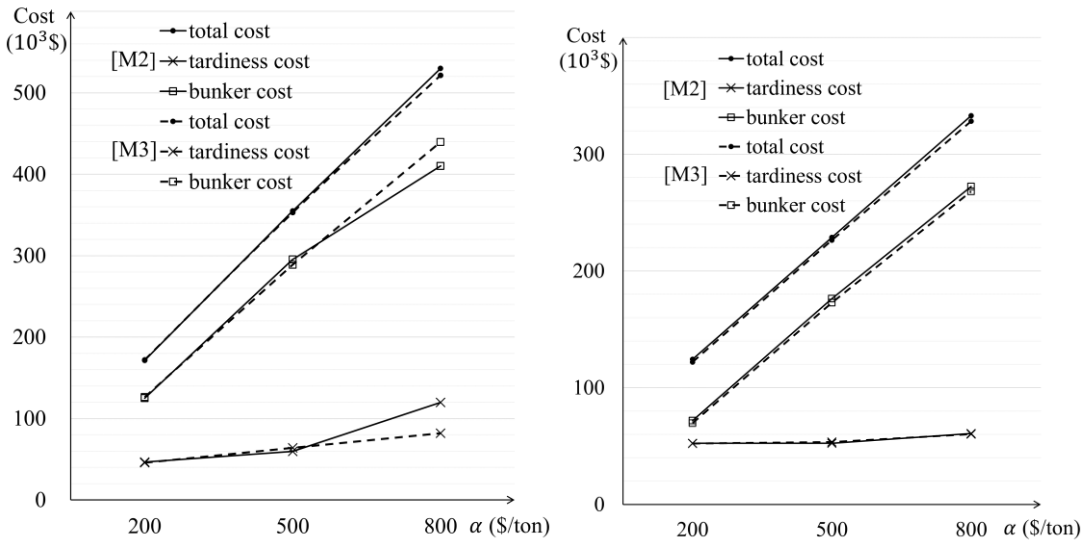

(a) Scenario 1 (b) Scenario 2

Fig. 5. Total cost and cost components versus α.

We further examine the detailed solutions, i.e., the optimal λ_v, μ_v, and p_v, of [M2] and [M3]. For simplicity, only the results for Scenario 1 are plotted in Fig. 6a–c. Similar findings were also observed for Scenario 2 but are omitted here for simplicity. Note that the figures unveil a variety of mismatches between the solid curves (solutions from [M2]) and the dashed ones (solutions from [M3]), especially for vessel 9 when $\alpha = 800$ \$/ton (see the corresponding points in Fig. 6a and c). It is important to note that the figures reveal various discrepancies between the solid curves (solutions obtained from [M2]) and the dashed curves (solutions derived from [M3]), particularly for vessel 9 when α = 800 \$/ton (refer to the corresponding points in Fig. 6a and c). Despite the small ε and Δt used and the similarity in objective values, the two approximation models yielded considerably different solutions. This observation suggests the presence of significantly distinct near-optimal solutions with comparable objective values.

Fig. 6a–c also show that the sailing times and schedule delays of vessels 1–6 exhibit moderate sensitivity to α. Specifically, the delays tend to increase with α, as illustrated in Fig. 6c. On the other hand, the sailing times and delays of vessels 7–12 are insensitive to α, possibly because those vessels have larger penalty rates (see the bold curve in Fig. 6c). For the same

reason, the delays of vessels 7–12 are relatively low. (Vessel 9's delay in the [M2] solution for α=800 \$/ton is an exception, possibly due to the inaccuracy of the solution.)

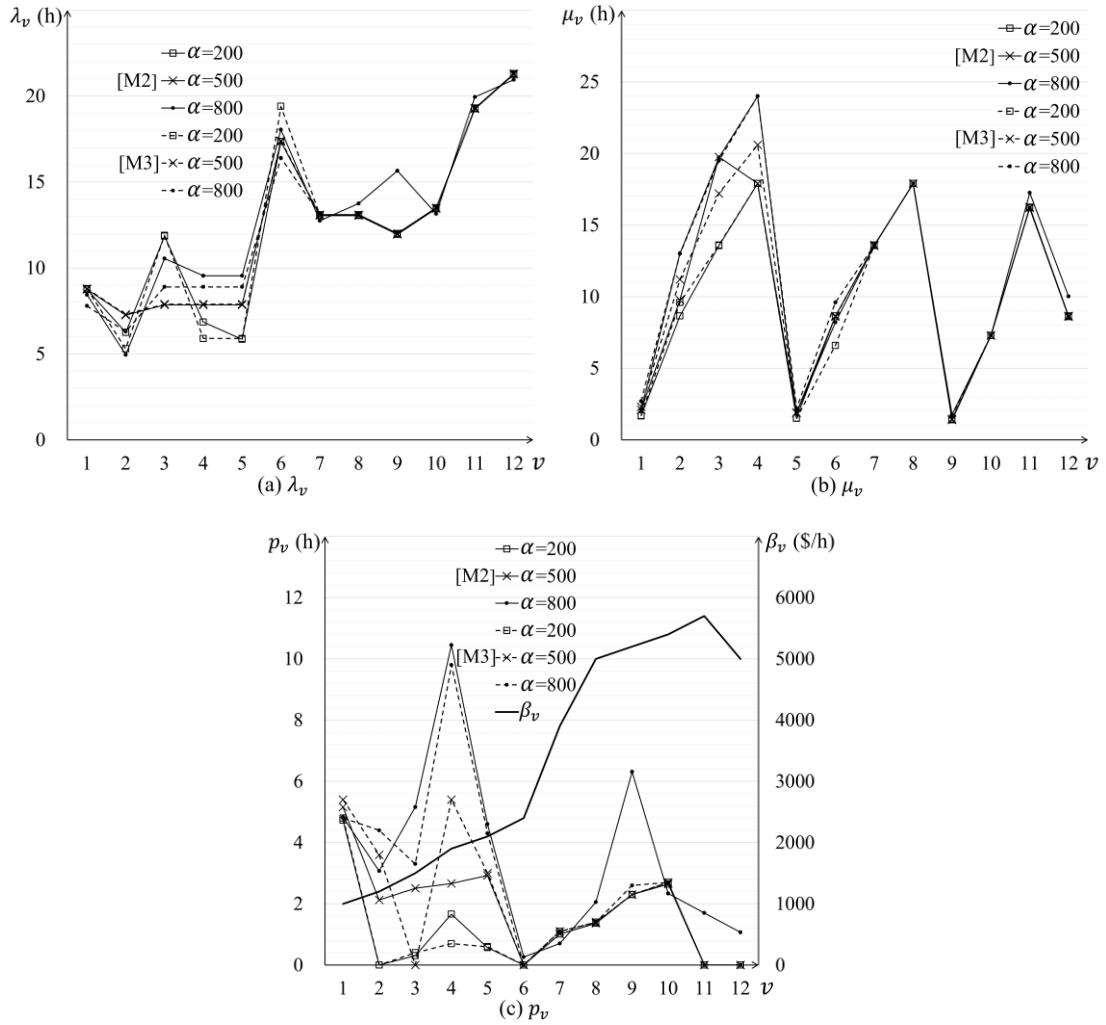

Fig. 6. Optimal vessel sailing times and delays under Scenario 1.

4.3 The benefit of optimal coordination

To better understand the benefit of optimal vessel scheduling, we compare the cost of optimal scheduling against two benchmark strategies.

The first strategy assumes no central operations manager, meaning that the individual vessels' sailing times are not coordinated. Each vessel optimizes its speed profile without knowing other vessels' arrival times at the bottleneck. When vessels form a queue at the bottleneck, they will pass following the first-come, first-serve (FCFS) rule. Each vessel will then re-optimize its speed for the second sailing leg after passing the bottleneck. The scheduling and cost evaluation model under this FCFS strategy is formulated in Appendix C.

The second strategy assumes that the central operations manager adopts a "naïve" rule to prioritize the vessels with higher penalty rates. Specifically, the manager sorts all the vessels according to their β_v's in descending order. (Thus, we term this strategy the descending-penalty or DP strategy.) The vessel with the maximum β_v will adopt a speed profile that minimizes its own cost. From the second vessel on, each vessel can pass the bottleneck following its cost-minimizing speed profile if the passage does not conflict with any vessel with a higher β_v. If a conflict occurs, that vessel will have to postpone its passage. After determining all the vessels' passage times at the bottleneck, the central operations manager will re-optimize their speeds to avoid queues. This strategy's scheduling and cost evaluation model is relegated to Appendix D.

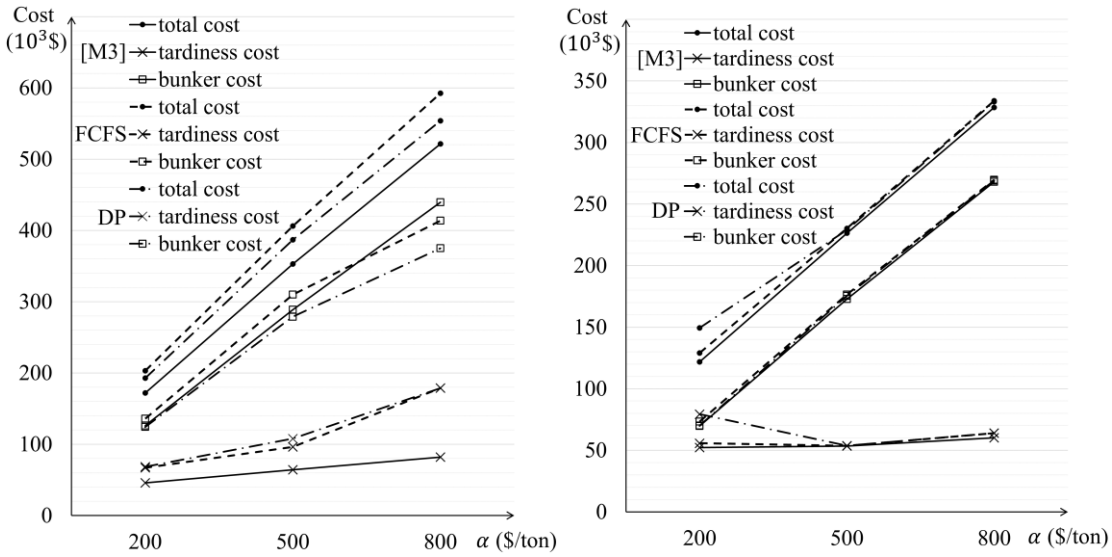

(a) Scenario 1 (b) Scenario 2

Fig. 7. Comparison of the three scheduling strategies.

We compare the total cost, the tardiness penalty, and the bunker cost under the optimal scheduling strategy, the FCFS strategy, and the DP strategy for the two scenarios of the TGD case in Fig. 7a and b. Only the solutions of [M3] are used for comparison because we reckon that they are more accurate than the [M2] solutions.

Fig. 7a shows that the optimal scheduling strategy can save up to 12% of the total cost compared to the FCFS strategy with no coordination and 5.8% compared to the DP strategy with naïve coordination. This manifests the considerable cost advantage of the system-optimal

coordination and scheduling. Further comparison of the cost components reveals that the tardiness penalty under the optimal strategy is much lower than the two benchmark strategies, which is the main reason for the cost advantage of optimal coordination.

To our surprise, the DP strategy exhibits the highest delay penalty but the lowest bunker cost. This is because some vessels with low penalty rates have to postpone their passages by much to make way for those with higher penalty rates, even if the latter vessels arrive at the bottleneck later. As a result, the DP strategy yields the longest schedule delays and the highest tardiness penalty, indicating that simply prioritizing vessels according to their penalty rates is ineffective. For the same reason, vessels under this strategy sail at slower speeds after the speed re-optimization, which leads to the lowest bunker cost.

On the other hand, Fig. 7b shows that the three strategies produce similar costs in Scenario 2 (only the cost under the DP strategy for $\alpha = 200$ \$/ton is moderately higher due to the relatively larger tardiness penalty). This is because most vessels suffer only small penalties due to their wide sailing time windows in Scenario 2, regardless of the strategy. Thus, the room for improvement by optimally coordinating vessel travel is meager.

5. Discussion of contributions, key findings, and their implications

First, this paper jointly optimizes heterogeneous vessels' sailing speeds and bottleneck passage schedules to minimize the total bunker cost and schedule delay penalty. Note that prior studies on sailing speed optimization did not account for queueing effects at waterway bottlenecks (Wang and Meng, 2012; Meng et al., 2015; Wen et al., 2016; Zhen et al., 2016), and research on ship queueing at bottlenecks largely overlooked the relationship between sailing speed and bunker cost (Hermans, 2014; Laih and Sun, 2014; Passchyn et al., 2016; Lalla-Ruiz et al., 2018; Hill et al., 2019; Deng et al., 2021). Furthermore, the nonlinear relationship between speed and bunker consumption highlights a fundamental distinction between vessel scheduling problems involving bottlenecks and roadway traffic bottleneck problems (see Section 1.2.1). The above underscores the unique contribution of our work within literature.

Methodologically, we compare the solution quality and computational cost of two widely-used linearization approaches (the outer-approximation method and the discrete-time method). Our results reveal that the latter method outperforms the former in terms of both solution quality and computational efficiency, especially for large-scale instances. This is partly due to the errors arising in the numerical computation of the tangent lines and points for [M2] (see Appendix A). These errors may increase as the predefined error bound ε diminishes, thus rendering the theoretical error bound invalid. The findings speak to the limitations of the former method and the advantages of the latter, offering valuable guidance for methodological choices in future studies addressing similar problems. Moreover, identifying tight bounds for decision variables is essential for enhancing computational efficiency (see Appendix B).

Our numerical case study demonstrates the sizeable benefits of system-optimal vessel scheduling. For instance, when considering the Three Gorges Dam case, the roughly estimated annual cost saving for all vessels traversing TGD amounts to approximately 97 million USD, compared against the default FCFS strategy.[3] The huge benefits highlight the importance of centralized vessel coordination. The benefits become greater when the vessels' sailing time windows are tighter (e.g., vessels carrying time-sensitive goods). Conversely, for vessels with flexible time windows or goods with low time values (e.g., certain types of bulk cargo), system-optimal scheduling offers relatively modest benefits, and the uncoordinated FCFS strategy is sufficiently effective.

A potential approach to implement the system-optimal scheduling strategy is to have the bottleneck management authority assume control over all vessel passages. This authority would determine the timing and sequence for each vessel's service at the bottleneck (similar to the role played by the Three Gorges Navigation Authority). The deployment of remotely-controlled autonomous ships (Akbar et al., 2021; Yang et al., 2023) in the future could also facilitate the execution of such strategies. Alternatively, if a central operations manager is not available,

[3] This is calculated by multiplying the average cost saving per vessel from the two scenarios examined in Section 4.3 by the 40,667 vessels that passed TGD in 2022 (Three Gorges Navigation Authority, 2023). The oil price is set at 550 $/ton (Ship and Bunker, 2023).

managerial strategies that approximate the system-optimal solution, such as pricing or tradable credit schemes, are worth exploring. This presents a potential direction for future research.

Our numerical results also unveil the impacts of key operating factors on optimal vessel scheduling. Particularly, both the total cost and tardiness penalty are sensitive to the bunker price. Regarding individual vessels, schedules of those with lower penalty rates (i.e., those carrying time-insensitive goods) are adjusted to counteract cost increases resulting from high bunker prices, while vessels carrying time-sensitive cargo are more likely to maintain their original schedules to avoid high tardiness penalties. Thus, when the oil price is high, policy makers can develop measures to promote fuel-efficient shipping, alternative fuels usage, or alternative transportation modes (e.g., trains) for time-sensitive goods.

6. Conclusions and future research

This paper presents a novel nonlinear model aimed at minimizing the sum of vessel bunker costs and lateness penalties by determining the system-optimal vessel schedules for navigating a shared bottleneck and their corresponding speed profiles. Two linear approximations for the model are proposed. The first utilizes a piecewise linear lower bound to approximate the nonlinear bunker consumption function, while the second transforms the original model into a binary integer program by discretizing time. A comparison between these two approximation methods demonstrates that the discrete-time model frequently yields superior solutions within a shorter time.

Our case study focuses on a real-world waterway bottleneck, the Three Gorges Dam Lock. The results reveal the influence of bunker prices, sailing time window tightness, and penalty rates on optimal vessel schedules and minimal costs. By comparing our strategy with a no-coordination strategy and a naïve coordination strategy, we demonstrate that system-optimal vessel scheduling can considerably reduce costs, particularly tardiness penalties when sailing time windows are tight. Insights are revealed and their implications on theory and practice are discussed.

A major limitation of our work is the assumption that a central operations manager has full control over all vessel itineraries. In the absence of such a manager, a "user equilibrium" model where vessels compete for bottleneck passage to minimize their individual costs is more realistic. This model can be formulated using a game theory framework. Furthermore, the model can be extended to examine the impact of policy instruments, such as pricing schemes (e.g., Zhuge et al., 2021; Hu et al., 2022), designed to encourage vessels towards specific forms of "coordination."

Other limitations include: neglecting emissions as an alternative objective, assuming the presence of a single bottleneck (whereas in some real cases, vessel navigation might be subject to multiple bottlenecks, such as a canal and a congested terminal), and overlooking the impact of water flow on vessel travel times. These limitations suggest potential future research directions, some of which are already being investigated. Future research will also be conducted on more realistic case studies and scheduling problems for vessels utilizing alternative fuels, such as battery-electric ships and fuel cell ships (Jimenez et al., 2022; Wu et al., 2022).

Acknowledgments

This study is supported by a General Research Fund (Project No. 15224818) provided by the Research Grants Council of Hong Kong and a start-up grant provided by the Hong Kong Polytechnic University (Project ID: P0001008).

Appendix A. The outer approximation and its computational limitation

First, divide the objective error bound ε (\$) by the fuel price α and the total distance traveled by all the vessels. This yields the error bound for each nautical mile traveled, denoted by $\bar{\varepsilon}$ (tons/n mile):

$$\bar{\varepsilon} = \frac{\varepsilon}{\alpha} \times \frac{1}{\sum_{v \in V}(L_{1v}+L_{2v})}. \quad \text{(A1)}$$

In what follows, we derive piecewise linear approximations $\bar{Q}_{1v}(\lambda_v)$ and $\bar{Q}_{2v}(\mu_v)$ ($\forall v \in V$) that satisfy:

$$|\bar{Q}_{1v}(\lambda_v) - Q_{1v}(\lambda_v)| \le \bar{\varepsilon}, |\bar{Q}_{2v}(\mu_v) - Q_{2v}(\mu_v)| \le \bar{\varepsilon}, \forall v \in V \quad \text{(A2)}$$

Note that $Q_{1v}(\lambda_v)$ and $Q_{2v}(\mu_v)$ represent the bunker consumption per nautical mile for vessel v's two sailing legs. Thus, Equation (A2) guarantees (theoretically) that the error in the bunker consumption cost is no greater than ε.

We next present an algorithm that generates a convex piecewise-linear function $\bar{Q}_{1v}(\lambda_v)$ with as few linear segments as possible. The algorithm for generating $\bar{Q}_{2v}(\mu_v)$ is similar and thus omitted for brevity.

The algorithm uses the first-order derivative of $Q_{1v}(\lambda_v)$ and the inverse of $Q_{1v}(\lambda_v)$. These are presented as follows:

$$Q'_{1v}(\lambda_v) = -a_v b_v {L_{1v}}^{b_v} (\lambda_v)^{-b_v - 1}, \forall v \in V \quad \text{(A3)}$$

$$Q_{1v}^{-1}(q) = L_{1v} \left(\frac{q}{a_v}\right)^{-\frac{1}{b_v}}, \forall v \in V. \quad \text{(A4)}$$

Since $Q_{1v}(\lambda_v)$ is a monotonically decreasing function, its inverse function exists and is also a decreasing function. Thus, $0 < Q_{1v}(\lambda_v) \le \bar{\varepsilon}$ if $\lambda_v \ge Q_{1v}^{-1}(\bar{\varepsilon})$. This condition means the approximation $\bar{Q}_{1v}(\lambda_v)$ can be set to zero when $\lambda_v \ge Q_{1v}^{-1}(\bar{\varepsilon})$; see Fig. A1.

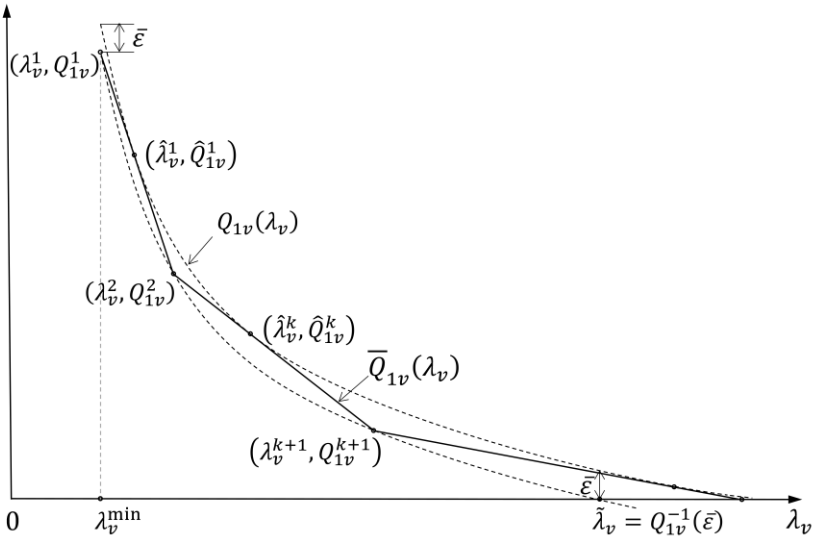

Fig. A1. Illustration of the piecewise linear approximation.

The algorithm is illustrated in Fig. A1. We start from a point that is $\bar{\varepsilon}$ below curve $Q_{1v}(\lambda_v)$ at the left end of the feasible range of λ_v, denoted by (λ_v^1, Q_{1v}^1) in the figure. Draw a tangent line from that point to curve $Q_{1v}(\lambda_v)$. End this line segment when the error from

$Q_{1v}(\lambda_v)$ increases to $\bar{\varepsilon}$ again, i.e., at point (λ_v^2, Q_{1v}^2). This tangent line will be the first one in the set of linear approximation functions. Similarly, draw the second tangent line to $Q_{1v}(\lambda_v)$ from point (λ_v^2, Q_{1v}^2). Repeat this process until $\lambda_v^k \geq \min\{Q_{1v}^{-1}(\bar{\varepsilon}), \lambda_v^{\max}\}$. If $\lambda_v^k < \lambda_v^{\max}$, add line $0 \cdot \lambda_v + 0$ to the set of linear approximation functions. Details of this algorithm are furnished below.

Algorithm 1: Generate a piecewise linear approximation of $Q_{1v}(\lambda_v)$ ($v \in V$)

Step 0: Denote Ω the set of approximation lines. Initialize $\Omega = \emptyset$. Define $\lambda_v^{\min} = L_{1v}/s_v^{\max}$, $\tilde{\lambda}_v = Q_{1v}^{-1}(\bar{\varepsilon})$, and $\lambda_v^{\max}$ by (10a). Set $k = 1$, $\lambda_v^k = \lambda_v^{\min}$, and $Q_{1v}^k = Q_{1v}(\lambda_v^k) - \bar{\varepsilon}$.

Step 1: Add to Ω the line (numbered line k) that passes point (λ_v^k, Q_{1v}^k) and is tangential to $Q_{1v}(\lambda_v)$. The point of tangency, denoted by $(\hat{\lambda}_v^k, \hat{Q}_{1v}^k)$, can be obtained by solving the following equation for $\hat{\lambda}_v^k$ (and $\hat{Q}_{1v}^k = Q_{1v}(\hat{\lambda}_v^k)$):

$$Q'_{1v}(\hat{\lambda}_v^k) = \frac{Q_{1v}(\hat{\lambda}_v^k) - Q_{1v}^k}{\hat{\lambda}_v^k - \lambda_v^k}. \tag{A5}$$

The equation of line k is given by:

$$Q_{1v} - Q_{1v}^k = Q'_{1v}(\hat{\lambda}_v^k)(\lambda_v - \lambda_v^k). \tag{A6}$$

Set $\theta_{1vk} = Q'_{1v}(\hat{\lambda}_v^k)$ and $\gamma_{1vk} = Q_{1v}^k - Q'_{1v}(\hat{\lambda}_v^k)\lambda_v^k$. Then Equation (A6) can be written as:

$$Q_{1v} = \theta_{1vk}\lambda_v + \gamma_{1vk}. \tag{A7}$$

Step 2: If the gap between line k and $Q_{1v}(\lambda_v)$ is not greater than $\bar{\varepsilon}$ when $\lambda_v = \min\{\tilde{\lambda}_v, \lambda_v^{\max}\}$, i.e.,

$$Q'_{1v}(\hat{\lambda}_v^k)(\min\{\tilde{\lambda}_v, \lambda_v^{\max}\} - \lambda_v^k) + Q_{1v}^k \geq Q_{1v}(\min\{\tilde{\lambda}_v, \lambda_v^{\max}\}) - \bar{\varepsilon}, \tag{A8}$$

go to Step 3.

Otherwise, there exists a unique point $(\lambda_v^{k+1}, Q_{1v}^{k+1})$ on line k, such that $\hat{\lambda}_v^k < \lambda_v^{k+1} < \min\{\tilde{\lambda}_v, \lambda_v^{\max}\}$ and $Q_{1v}^{k+1} = Q_{1v}(\lambda_v^{k+1}) - \bar{\varepsilon}$. The λ_v^{k+1} can be obtained by solving the following equation:

$$Q_{1v}(\lambda_v^{k+1}) - \bar{\varepsilon} - Q_{1v}^k = Q'_{1v}(\hat{\lambda}_v^k)(\lambda_v^{k+1} - \lambda_v^k). \tag{A9}$$

Set $k = k + 1$ and go to Step 1.

Step 3: Set $K_{1v} = k$. The $\overline{Q}_{1v}(\lambda_v)$ is defined by:

$$\overline{Q}_{1v}(\lambda_v) = \max\{0, \theta_{1vk}\lambda_v + \gamma_{1vk}, k = 1,2,\cdots,K_{1v}\}. \tag{A10}$$

However, numerical errors arise in the above process, especially when solving Equation (A5) in Algorithm 1 for the point of tangency $(\hat{\lambda}_v^k, \hat{Q}_{1v}^k)$. Inspection of Fig. A1 reveals that the

error would be relatively large under two conditions: (i) where the first-order derivative of the original bunker consumption function, $Q'_{1v}(\lambda_v)$, changes slowly, or equivalently, where $Q''_{1v}(\lambda_v)$ is small; and (ii) where the start point of the tangent line, (λ_v^k, Q_{1v}^k), is close to curve $Q_{1v}(\lambda_v)$. Unfortunately, both conditions are satisfied for our bunker consumption function. Condition (ii) becomes stronger when the predefined error bound ε is smaller. Moreover, the error in $(\hat{\lambda}_v^k, \hat{Q}_{1v}^k)$ would be amplified by the extrapolation for calculating $(\lambda_v^{k+1}, Q_{1v}^{k+1})$, the start of the next linear segment. Hence, the resulting approximation error may exceed the theoretical bound ε, and it may not diminish as ε approaches zero. This could explain why the solution quality of [M2] does not match the expectation in Section 3.

Appendix B. Proof of (10a–b)

We first prove that (10a) is an upper bound of the optimal λ_v.

Denote $c_v(\lambda_v, \mu_v) = \alpha[L_{1v}Q_{1v}(\lambda_v) + L_{2v}Q_{2v}(\mu_v)] + \beta_v p_v$ the total bunker consumption and penalty cost for vessel $v \in V$. We next examine the value of λ_v that minimizes $c_v(\lambda_v, \mu_v)$. To this end, we consider that μ_v is fixed for now.

First, when $\lambda_v \leq -T_v^0 - \omega - \mu_v + T_v$, $p_v = 0$; see (4a) and (6e). In this case, $c_v(\lambda_v, \mu_v)$ is decreasing with λ_v because $Q_{1v}(\lambda_v)$ is a decreasing function of λ_v; see (7a).

On the other hand, when $\lambda_v > -T_v^0 - \omega - \mu_v + T_v$, $p_v = T_v^0 + \lambda_v + \omega + \mu_v - T_v$ which increases linearly with λ_v. Now $c_v(\lambda_v, \mu_v)$ becomes:

$$c_v(\lambda_v, \mu_v) = \alpha[L_{1v}Q_{1v}(\lambda_v) + L_{2v}Q_{2v}(\mu_v)] + \beta_v(T_v^0 + \lambda_v + \omega + \mu_v - T_v), \text{if } \lambda_v > -T_v^0 - \omega - \mu_v + T_v. \quad \text{(B1)}$$

The partial derivative of $c_v(\lambda_v, \mu_v)$ on λ_v is given by:

$$\frac{\partial c_v}{\partial \lambda_v} = \alpha L_{1v} Q'_{1v}(\lambda_v) + \beta_v = -\frac{\alpha a_v b_v {L_{1v}}^{b_v+1}}{(\lambda_v)^{b_v+1}} + \beta_v. \quad \text{(B2)}$$

Moreover, the second-order partial derivative of $c_v(\lambda_v, \mu_v)$ on λ_v is:

$$\frac{\partial^2 c_v}{\partial \lambda_v^2} = \frac{\alpha a_v b_v (b_v+1) {L_{1v}}^{b_v+1}}{(\lambda_v)^{b_v+2}} > 0 \quad \text{(B3)}$$

Thus, when $\lambda_v > -T_v^0 - \omega - \mu_v + T_v$ and μ_v is fixed, $c_v(\lambda_v, \mu_v)$ is convex for λ_v and is minimized when $\frac{\partial c_v}{\partial \lambda_v} = 0$. This yields $\bar{\lambda}_v = L_{1v}\left(\frac{\alpha a_v b_v}{\beta_v}\right)^{\frac{1}{b_v+1}}$. Combining the monotonically decreasing segment of $c_v(\lambda_v, \mu_v)$ when $\lambda_v \leq -T_v^0 - \omega - \mu_v + T_v$ and the convex segment when $\lambda_v > -T_v^0 - \omega - \mu_v + T_v$, we have:

$$\bar{\bar{\lambda}}_v = \max\left\{T_v - T_v^0 - \omega - \mu_v, L_{1v}\left(\frac{\alpha a_v b_v}{\beta_v}\right)^{\frac{1}{b_v+1}}\right\}. \quad \text{(B4)}$$

This is the value of λ_v that minimizes $c_v(\lambda_v, \mu_v)$ for a given μ_v. It is thus the optimal λ_v for vessel v if the interactions between vessels at the bottleneck are ignored and μ_v is given. Considering that $\mu_v \geq \frac{L_{2v}}{s_v^{\max}}$, any value of λ_v that is greater than the following bound will only increase vessel v's cost:

$$\bar{\bar{\lambda}}_v^{\max} = \max\left\{T_v - T_v^0 - \omega - \frac{L_{2v}}{s_v^{\max}}, L_{1v}\left(\frac{\alpha a_v b_v}{\beta_v}\right)^{\frac{1}{b_v+1}}\right\}. \quad \text{(B5)}$$

Now consider the interactions between vessels. Vessel v may not be able to pass the bottleneck at its own cost-minimizing time $\bar{\bar{\lambda}}_v$ (which is capped by $\bar{\bar{\lambda}}_v^{\max}$) because it may have to make way for other vessels. We consider a worst-case scenario, where the present vessel v must make way for all the other $|V| - 1$ vessels. Moreover, the other $|V| - 1$ vessels arrive at the bottleneck at $\bar{\bar{\lambda}}_v + H - \hat{\epsilon}$, $\bar{\bar{\lambda}}_v + 3H - 2\hat{\epsilon}$, $\bar{\bar{\lambda}}_v + 5H - 3\hat{\epsilon}$, …, $\bar{\bar{\lambda}}_v + (H - \hat{\epsilon}) + (2H - \hat{\epsilon})(|V| - 2)$, where $\hat{\epsilon}$ is a very small positive value. In this case, vessel v cannot pass the bottleneck between $\bar{\bar{\lambda}}_v$ and $\bar{\bar{\lambda}}_v + (2H - \hat{\epsilon})(|V| - 1)$ without delaying other vessels. In other words, it must pass the bottleneck either before $\bar{\bar{\lambda}}_v$ or after $\bar{\bar{\lambda}}_v + (2H - \hat{\epsilon})(|V| - 1)$. Since $\bar{\bar{\lambda}}_v + (2H - \hat{\epsilon})(|V| - 1) < \bar{\bar{\lambda}}_v + 2(|V| - 1)H \leq \bar{\bar{\lambda}}_v^{\max} + 2(|V| - 1)H$, any value of λ_v greater than $\bar{\bar{\lambda}}_v^{\max} + 2(|V| - 1)H$ will be suboptimal.

Finally, it is obvious that $\lambda_v^{\max} \geq \frac{L_{1v}}{s_v^{\max}}$. Combining the above results, we have:

$$\lambda_v^{\max} = \max\left\{\max\left\{T_v - T_v^0 - \omega - \frac{L_{2v}}{s_v^{\max}}, L_{1v}\left(\frac{\alpha a_v b_v}{\beta_v}\right)^{\frac{1}{b_v+1}}\right\} + 2(|V| - 1)H, \frac{L_{1v}}{s_v^{\max}}\right\}, \forall v \in V, \quad \text{(B6)}$$

which is (10a).

Upper bound (10b) can be proved similarly. The only difference is that vessel v does not need to make way for other vessels after passing the bottleneck. Thus, term $2(|V|-1)H$ in (B6) will not appear in the upper bound of the optimal μ_v.

Appendix C. FCFS scheduling strategy

The vessel scheduling solution and the associated cost under the FCFS strategy are formulated in three steps.

Step 1 minimizes each vessel v's schedule regardless of the minimum headway constraint. The model is denoted by [M4-v] for vessel $v \in V$:

[M4-v]

$$\min c(\lambda_v, \mu_v) = \alpha \left[L_{1v} a_v \left(\frac{L_{1v}}{\lambda_v}\right)^{b_v} + L_{2v} a_v \left(\frac{L_{2v}}{\mu_v}\right)^{b_v} \right] + \beta_v \tag{C1a}$$

subject to

$$p_v = \max\{0, T_v^0 + \lambda_v + \omega + \mu_v - T_v\} \tag{C1b}$$

$$\lambda_v \geq \frac{L_{1v}}{s_v^{\max}} \tag{C1c}$$

$$\mu_v \geq \frac{L_{2v}}{s_v^{\max}}. \tag{C1d}$$

[M4-v] can be solved analytically. From the analysis in Appendix B, we know that for a fixed μ_v, the optimal λ_v is:

$$\lambda_v^*(\mu_v) = \max\left\{ T_v - (T_v^0 + \omega + \mu_v), L_{1v} \left(\frac{\alpha a_v b_v}{\beta_v}\right)^{\frac{1}{b_v+1}}, \frac{L_{1v}}{s_v^{\max}} \right\}. \tag{C2}$$

For simplicity, we define $\tilde{\lambda}_v = \max\left\{ L_{1v} \left(\frac{\alpha a_v b_v}{\beta_v}\right)^{\frac{1}{b_v+1}}, \frac{L_{1v}}{s_v^{\max}} \right\}$ and $\tilde{T}_v = T_v - (T_v^0 + \omega)$. Thus, $\lambda_v^*(\mu_v)$ is simplified as:

$$\lambda_v^*(\mu_v) = \max\{\tilde{T}_v - \mu_v, \tilde{\lambda}_v\}. \tag{C3a}$$

Note that if we swap λ_v with μ_v and L_{1v} with L_{2v} in (C1a–d), the formulation remains the same. Thus, we can similarly write the optimal μ_v as a function of λ_v:

$$\mu_v^*(\lambda_v) = \max\{\tilde{T}_v - \lambda_v, \tilde{\mu}_v\}. \tag{C3b}$$

where $\tilde{\mu}_v = \max\left\{L_{2v}\left(\frac{\alpha a_v b_v}{\beta_v}\right)^{\frac{1}{b_v+1}}, \frac{L_{2v}}{s_v^{\max}}\right\}$.

Combining (C3a–b), we consider the following two cases illustrated in Fig. C1a and b.

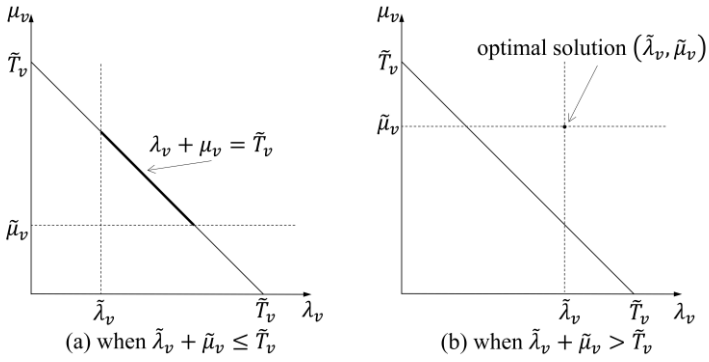

Fig. C1. Illustration of the two cases.

Case 1: when $\tilde{\lambda}_v + \tilde{\mu}_v \le \tilde{T}_v$ (Fig. C1a). The reader can verify that the optimal solution of (λ_v, μ_v) satisfying (C3a–b) must lie in the red line segment in Fig. C1a, which is described by: $\lambda_v + \mu_v = \tilde{T}_v,\ \tilde{\lambda}_v \le \lambda_v \le \tilde{T}_v - \tilde{\mu}_v$. In this case, $p_v = 0$. Thus,

$$c(\lambda_v, \mu_v) \equiv \tilde{c}(\lambda_v) = \alpha a_v \left[L_{1v}\left(\frac{L_{1v}}{\lambda_v}\right)^{b_v} + L_{2v}\left(\frac{L_{2v}}{\tilde{T}_v - \lambda_v}\right)^{b_v}\right]. \tag{C4}$$

The first- and second-order derivatives of $\tilde{c}(\lambda_v)$ are:

$$\frac{d\tilde{c}}{d\lambda_v} = \alpha a_v \left[-b_v L_{1v}^{b_v+1}\lambda_v^{-b_v-1} + b_v L_{2v}^{b_v+1}\left(\tilde{T}_v - \lambda_v\right)^{-b_v-1}\right] \tag{C5}$$

$$\frac{d^2\tilde{c}}{d\lambda_v^2} = \alpha a_v \left[b_v(b_v+1)L_{1v}^{b_v+1}\lambda_v^{-b_v-2} + b_v(b_v+1)L_{2v}^{b_v+1}\left(\tilde{T}_v - \lambda_v\right)^{-b_v-2}\right] > 0. \tag{C6}$$

Thus, $\tilde{c}(\lambda_v)$ is a convex function whose minimizer can be derived by letting $\frac{d\tilde{c}}{d\lambda_v} = 0$:

$$\hat{\lambda}_v = \frac{L_{1v}\tilde{T}_v}{L_{1v}+L_{2v}}. \tag{C7}$$

Considering the boundary constraint $\tilde{\lambda}_v \le \lambda_v \le \tilde{T}_v - \tilde{\mu}_v$, the optimal solution to (C1a–d) is:

$$\begin{cases} \lambda_v^* = \mathrm{mid}\left(\tilde{\lambda}_v, \hat{\lambda}_v, \tilde{T}_v - \tilde{\mu}_v\right) \\ \mu_v^* = \tilde{T}_v - \lambda_v^* \end{cases}, \tag{C8}$$

where function $\mathrm{mid}(\cdot)$ returns the middle one of the three arguments.

Case 2: when $\tilde{\lambda}_v + \tilde{\mu}_v > \tilde{T}_v$ (Fig. C1b). The reader can verify that there exists a unique optimal solution satisfying (C3a–b): $(\lambda_v^*, \mu_v^*) = \left(\tilde{\lambda}_v, \tilde{\mu}_v\right)$.

From the optimal solution (λ_v^*, μ_v^*), we derive the vessels' arrival time at the bottleneck, $\bar{x}_v = T_v^0 + \lambda_v^*, \forall v \in V$.

Step 2: Sort $\{\bar{x}_v, v \in V\}$ in ascending order. Denote the sorted sequence by $\{\bar{x}_{(i)}\}$, i.e., $\bar{x}_{(1)} \leq \bar{x}_{(2)} \leq \cdots \leq \bar{x}_{(|V|)}$. Incorporate constraints (2d) in the following way. Define a new sequence $\{\tilde{x}_{(i)}\}$ such that $\tilde{x}_{(1)} = \bar{x}_{(1)}$ and $\tilde{x}_{(i+1)} = \max\{\bar{x}_{(i+1)}, \tilde{x}_{(i)} + H\}$, $\forall i \in \{1,2,\dots,|V|-1\}$. Note that $\{\bar{x}_v\}$ indicate the vessels' desired passage times while $\{\tilde{x}_{(i)}\}$ represent their actual passage times considering the minimum headway H.

Step 3: Given the updated vessel arrival times at the bottleneck, $\{\tilde{x}_{(i)}\}$, re-optimize μ_v for each vessel $v \in V$ using the following model denoted by [M5-v]:

[M5-v]

$$\min \alpha L_{2v} a_v \left(\frac{L_{2v}}{\mu_v}\right)^{b_v} + \beta_v p_v \tag{C9a}$$

subject to

$$p_v = \max\{0, \tilde{x}_v + \omega + \mu_v - T_v\} \tag{C9b}$$

$$\mu_v \geq \frac{L_{2v}}{s_v^{\max}}. \tag{C9c}$$

where $\tilde{x}_v$ is obtained from $\{\tilde{x}_{(i)}\}$. [M5-v] can be simply solved using (C3b) by letting $\lambda_v = \tilde{x}_v - T_v^0$. Denote the optimal solution of [M5-v] by μ_v^{**} and the corresponding delay by p_v^{**}.

Given the above solution, calculate the total cost by: $\sum_{v \in V} \left\{\alpha \left[L_{1v} a_v \left(\frac{L_{1v}}{\lambda_v^*}\right)^{b_v} + L_{2v} a_v \left(\frac{L_{2v}}{\mu_v^{**}}\right)^{b_v}\right] + \beta_v p_v^{**}\right\}$. Note in the FCFS solution that $\tilde{x}_v$ is not always equal to $T_v^0 + \lambda_v^*$ ($v \in V$). When the two are not equal, the difference is vessel v's waiting time at the bottleneck.

Appendix D. DP scheduling strategy

The vessel scheduling solution and the total cost under the DP strategy are also derived in three steps.

Step 1 is the same as Step 1 of the FCFS strategy (see Appendix C), which solves [M4-v] for each vessel $v \in V$ and calculates its arrival time at the bottleneck, $\bar{x}_v$.

Step 2: Adjust the vessel schedules in the descending penalty order to ensure constraints (2d) are satisfied.

Step 2.1: Sort the penalty rates $\{\beta_v, v \in V\}$ in descending order. Denote the resulting sequence by $\{\beta_{[i]}, i = 1,2, \dots, |V|\}$, i.e., $\beta_{[1]} \geq \beta_{[2]} \geq \cdots \geq \beta_{[|V|]}$. Write the corresponding sequence of $\bar{x}_v$ as $\{\bar{x}_{[i]}, i = 1,2, \dots, |V|\}$.

Step 2.2: Denote $\tilde{x}_{[i]}$ the actual arrival time of vessel $[i]$ at the bottleneck under the DP strategy. Initialize $\tilde{x}_{[i]} = \bar{x}_{[i]}$, $\forall i \in \{2,3, \dots, |V|\}$. Set $m = 2$.

Step 2.3: Find $l, n < m$ such that $l = \arg\max_{i<m}\{\tilde{x}_{[i]} | \tilde{x}_{[i]} \leq \tilde{x}_{[m]}\}$ and $n = \arg\min_{i<m}\{\tilde{x}_{[i]} | \tilde{x}_{[i]} \geq \tilde{x}_{[m]}\}$. Define $\Delta_1 = \tilde{x}_{[m]} - \tilde{x}_{[l]}$ and $\Delta_2 = \tilde{x}_{[n]} - \tilde{x}_{[m]}$. If l does not exist (i.e., $\tilde{x}_{[m]} < \tilde{x}_{[i]}, \forall i < m$), set $\Delta_1 = \infty$; and if n does not exist (i.e., $\tilde{x}_{[m]} > \tilde{x}_{[i]}, \forall i < m$), set $\Delta_2 = \infty$.

Step 2.4: Consider the following four cases regarding Δ_1 and Δ_2.

Case 1: $\Delta_1, \Delta_2 \geq H$. Set $m \leftarrow m + 1$. If $m > |V|$, go to **Step 3**. Otherwise, return to **Step 2.3**.

Case 2: $\Delta_1 < H$ and $\Delta_1 + \Delta_2 \geq 2H$. Set $\tilde{x}_{[m]} = \tilde{x}_{[l]} + H$. Set $m \leftarrow m + 1$. If $m > |V|$, go to **Step 3**. Otherwise, return to **Step 2.3**.

Case 3: $\Delta_1 < H$ and $\Delta_1 + \Delta_2 < 2H$. Set $\tilde{x}_{[m]} = \tilde{x}_{[n]} + H$. Return to **Step 2.3**.

Case 4: $\Delta_1 \geq H$ and $\Delta_2 < H$. Set $\tilde{x}_{[m]} = \tilde{x}_{[n]} + H$. Return to **Step 2.3**.

Step 3: Given the updated vessel arrival times at the bottleneck, $\{\tilde{x}_{[i]}\}$, re-optimize μ_v for each vessel $v \in V$ using [M5-v] in Appendix C. Calculate vessel v's arrival time $\tilde{y}_v$, $\forall v \in V$. Calculate the total cost under the DP strategy using (2a).

Under the DP strategy, the vessels experience no waiting time because the central operations manager will determine each vessel's speed profile and arrival time at the bottleneck.

References

Akbar, A., Aasen, A. K. A., Msakni, M. K., Fagerholt, K., Lindstad, E., Meisel, F., 2021. An economic analysis of introducing autonomous ships in a short-sea liner shipping network. *International Transactions in Operational Research*, 28(4), 1740–1764.

Andersson, H., Fagerholt, K., Hobbesland, K., 2015. Integrated maritime fleet deployment and speed optimization: Case study from RoRo shipping. *Computers & Operations Research*, 55, 233–240.

Arnott, R., de Palma, A., Lindsey, R., 1993. A structural model of peak-period congestion: A traffic bottleneck with elastic demand. *The American Economic Review*, 83(1), 161–179.

Chen, H., Liu, Y., Nie, Y. M., 2015. Solving the step-tolled bottleneck model with general user heterogeneity. *Transportation Research Part B: Methodological*, 81, 210–229.

Chen, J., Ye, J., Zhuang, C., Qin, Q., Shu, Y., 2022. Liner shipping alliance management: Overview and future research directions. *Ocean & Coastal Management*, 219, 106039.

Chen, J., Zhuang, C., Yang, C., Wan, Z., Zeng, X., Yao, J., 2021. Fleet co-deployment for liner shipping alliance: Vessel pool operation with uncertain demand. *Ocean & Coastal Management*, 214, 105923.

Cheng, Q., Liu, Z., Guo, J., Wu, X., Pendyala, R., Belezamo, B., Zhou, X. S., 2022. Estimating key traffic state parameters through parsimonious spatial queue models. *Transportation Research Part C: Emerging Technologies*, 137, 103596.

Christiansen, M., Fagerholt, K., Ronen, D., 2004. Ship routing and scheduling: Status and perspectives. *Transportation Science*, 38(1), 1–18.

Connolly, M., 2021. Panama Canal delays near 10 days. Available: https://www.argusmedia.com/en/news/2203100-panama-canal-delays-near-10-days [Accessed November 1, 2021].

Deng, Y., Sheng, D., Liu, B., 2021. Managing ship lock congestion in an inland waterway: A bottleneck model with a service time window. *Transport Policy*, 112, 142–161.

Dere, C., Deniz, C., 2019. Load optimization of central cooling system pumps of a container ship for the slow steaming conditions to enhance the energy efficiency. *Journal of Cleaner Production*, 222, 206–217.

de Palma, A., Lefèvre, C., 2019. *Bottleneck models and departure time problems*. Springer International Publishing.

Du, Y., Chen, Q., Quan, X., Long, L., Fung, R. Y., 2011. Berth allocation considering fuel consumption and vessel emissions. *Transportation Research Part E: Logistics and Transportation Review*, 47(6), 1021–1037.

Feng, X., Hu, S., Gu, W., Jin, X., Lu, Y., 2020. A simulation-based approach for assessing seaside infrastructure improvement measures for large marine crude oil terminals. *Transportation Research Part E: Logistics and Transportation Review*, 142, 102051.

Feng, X., Wang, M., Li, Y., Gu, W., Zhang, Y., 2015. Optimal throughput of crude oil terminals with options for infrastructure improvements. *Journal of Coastal Research* 73, 628-634.

Goicoechea, N., Abadie, L. M., 2021. Optimal slow steaming speed for container ships under the eu emission trading system. Energies, 14(22), 7487.

Golias, M. M., Saharidis, G. K., Boile, M., Theofanis, S., Ierapetritou, M. G., 2009. The berth allocation problem: Optimizing vessel arrival time. *Maritime Economics & Logistics*, 11(4), 358–377.

Gu, W., Ouyang, Y., Madanat, S., 2012. Joint optimization of pavement maintenance and resurfacing planning. *Transportation Research Part B: Methodological*, 46(4), 511–519.

Hermans, J., 2014. Optimization of inland shipping: A polynomial time algorithm for the single-ship single-lock optimization problem. *Journal of Scheduling*, 17(4), 305–319.

Hill, A., Lalla-Ruiz, E., Voß, S., Goycoolea, M., 2019. A multi-mode resource-constrained project scheduling reformulation for the waterway ship scheduling problem. *Journal of scheduling*, 22(2), 173–182.

Hu, Q., Gu, W., Wang, S., 2022. Optimal subsidy scheme design for promoting intermodal freight transport. *Transportation Research Part E: Logistics and Transportation Review*, 157, 102561.

Huang, L., Tan, Y., Guan, X., 2022. Hub-and-spoke network design for container shipping considering disruption and congestion in the post COVID-19 era. *Ocean & Coastal Management*, 225, 106230.

Karsten, C. V., Ropke, S., Pisinger, D., 2018. Simultaneous optimization of container ship sailing speed and container routing with transit time restrictions. *Transportation Science*, 52(4), 769–787.

Jimenez, V. J., Kim, H., Munim, Z. H., 2022. A review of ship energy efficiency research and directions towards emission reduction in the maritime industry. *Journal of Cleaner Production*, 366, 132888.

Laih, C.-H., Sun, P.-Y., 2014. The optimal toll scheme for ships queuing at the entrance of Panama Canal. *Maritime Economics & Logistics*, 16(1), 20–32.

Laih, C.-H., Tsai, Y.-C., Chen, Z.-B., 2015. Optimal non-queuing pricing for the Suez Canal. *Maritime Economics & Logistics*, 17(3), 359–370.

Lalla-Ruiz, E., Shi, X., Voß, S., 2018. The waterway ship scheduling problem. *Transportation Research Part D: Transport and Environment*, 60, 191–209.

LaRocco, L. A., 2021. Suez Canal blockage is delaying an estimated $400 million an hour in goods. Available: https://www.cnbc.com/2021/03/25/suez-canal-blockage-is-delaying-an-estimated-400-million-an-hour-in-goods.html [Accessed November 1, 2021].

Lave, L. B., DeSalvo, J. S., 1968. Congestion, tolls, and the economic capacity of a waterway. *Journal of Political Economy*, 76(3), 375–391.

Li, Z. C., Huang, H. J., Yang, H., 2020. Fifty years of the bottleneck model: A bibliometric review and future research directions. *Transportation research part B: methodological*, 139, 311–342.

Li, Z. C., Lam, W. H. K., Wong, S. C., 2017. Step tolling in an activity-based bottleneck model. *Transportation Research Part B: Methodological*, 101, 306–334.

Lin, H., Zeng, W., Luo, J., Nan, G., 2022. An analysis of port congestion alleviation strategy based on system dynamics. *Ocean & Coastal Management*, 229, 106336.

Liu, Y., Zhao, X., Huang, R., 2022. Research on comprehensive recovery of liner schedule and container flow with hard time windows constraints. *Ocean & Coastal Management*, 224, 106171.

Meisel, F., Fagerholt, K., 2019. Scheduling two-way ship traffic for the Kiel Canal: Model, extensions and a matheuristic. *Computers & Operations Research*, 106, 119–132.

Meng, Q., Wang, S., Andersson, H., Thun, K., 2014. Containership routing and scheduling in liner shipping: Overview and future research directions. *Transportation Science*, 48(2), 265–280.

Meng, Q., Wang, S., Lee, C.-Y., 2015. A tailored branch-and-price approach for a joint tramp ship routing and bunkering problem. *Transportation Research Part B: Methodological*, 72, 1–19.

Miller, G., 2020. How the Panama Canal traffic jam is affecting ocean shipping. Available: https://www.freightwaves.com/news/how-the-panama-canal-traffic-jam-is-affecting-ocean-shipping [Accessed November 1, 2021].

Notteboom, T. E., 2006. The time factor in liner shipping services. *Maritime Economics & Logistics*, 8(1), 19–39.

Passchyn, W., Coene, S., Briskorn, D., Hurink, J. L., Spieksma, F. C. R., Vanden Berghe, G., 2016. The lockmaster's problem. *European Journal of Operational Research*, 251(2), 432–441.

Pomfret, R., 2019. The Eurasian Land Bridge: Linking regional value chains along the New Silk Road. *Cambridge Journal of Regions, Economy & Society*, 12(1), 45–56.

Psaraftis, H. N., 2019. Ship routing and scheduling: The cart before the horse conjecture. *Maritime Economics & Logistics*, 21(1), 111–124.

Rogers, H., 2018. Panama Canal and LNG: Congestion Ahead? Available: https://www.oxfordenergy.org/wpcms/wp-content/uploads/2018/04/Panama-Canal-and-LNG-%E2%80%93-Congestion-Ahead-Insight-33.pdf [Accessed November 1, 2021].

Ronen, D., 1983. Cargo ships routing and scheduling: Survey of models and problems. *European Journal of Operational Research*, 12(2), 119–126.

Ronen, D., 2011. The effect of oil price on containership speed and fleet size. *Journal of the Operational Research Society*, 62(1), 211–216.

Rusinov, I., Gavrilova, I., Sergeev, M., 2021. Features of sea freight through the Suez Canal. *Transportation Research Procedia*, 54, 719–725.

Schoeneich, M., Habel, M., Szatten, D., Absalon, D., Montewka, J., 2023. An integrated approach to an assessment of bottlenecks for navigation on riverine waterways. *Water*, 15(1), 141.

Ship and Bunker, 2023. Global Average Bunker Prices. Available: https://shipandbunker.com/prices/av/global/av-g04-global-4-ports-average [Accessed May 11, 2023].

Sina News, 2020. It takes three hours to pass the lock of the Three Gorges Dam, so where is the time spent! Available: http://k.sina.com.cn/article_6427581697_m17f1d1d0100100qtis.html?sudaref=www.baidu.com&display=0&retcode=0 [Accessed November 1, 2021].

Small, K. A., 2015. The bottleneck model: An assessment and interpretation. *Economics of Transportation*, 4(1), 110–117.

Szeto, W. Y., Lo, H. K., 2005. The impact of advanced traveler information services on travel time and schedule delay costs. *Journal of Intelligent Transportation Systems*, 9(1), 47–55.

Tan, Z., Wang, Y., Meng, Q., Liu, Z., 2018. Joint ship schedule design and sailing speed optimization for a single inland shipping service with uncertain dam transit time. *Transportation Science*, 52(6), 1570–1588.

Three Gorges Navigation Authority, 2023. Navigation Situation in the Three Gorges Dam Area in December 2022. Available: https://sxth.mot.gov.cn/sj/sxthxsfx/202301/t20230116_288500.html [Accessed May 11, 2023].

Tian, L. J., Yang, H., Huang, H. J., 2013. Tradable credit schemes for managing bottleneck congestion and modal split with heterogeneous users. *Transportation Research Part E: Logistics and Transportation Review*, 54, 1–13.

UNCTAD, 2020. Review of Maritime Transport 2020. United Nations Conference on Trade and Development. Available: https://unctad.org/system/files/official-document/rmt2020_en.pdf [Accessed November 1, 2021].

Vickrey, W. S., 1969. Congestion theory and transport investment. *The American Economic Review*, 59(2), 251–260.

von Westarp, A. G., 2020. A new model for the calculation of the bunker fuel speed–consumption relation. *Ocean Engineering*, 204, 107262.

Wang, S., Meng, Q., 2012. Sailing speed optimization for container ships in a liner shipping network. *Transportation Research Part E: Logistics and Transportation Review*, 48(3), 701–714.

Wang, S., Meng, Q., Liu, Z., 2013. Bunker consumption optimization methods in shipping: A critical review and extensions. *Transportation Research Part E: Logistics and Transportation Review*, 53, 49–62.

Wardrop, J. G., 1952. Road paper. some theoretical aspects of road traffic research. *Proceedings of the Institution of Civil Engineers*, 1(3), 325–378.

Wen, M., Ropke, S., Petersen, H. L., Larsen, R., Madsen, O. B. G., 2016. Full-shipload tramp ship routing and scheduling with variable speeds. *Computers & Operations Research*, 70, 1–8.

WTO, 2021. Global trade rebound beats expectations but marked by regional divergences. World Trade Organization. Available: https://www.wto.org/english/news_e/pres21_e/pr889_e.htm [Accessed November 26, 2021].

Wu, Y., Huang, Y., Wang, H., Zhen, L., 2022. Joint planning of fleet deployment, ship refueling, and speed optimization for dual-fuel ships considering methane slip. *Journal of Marine Science and Engineering*, 10(11), 1690.

Xiao, F., Zhang, H. M., 2013. Pareto-improving and self-sustainable pricing for the morning commute with nonidentical commuters. *Transportation Science*, 48(2), 159–169.

Yang, X., Gu, W., Wang, W., Wang, S., 2023. Optimal scheduling of autonomous vessel trains in a hub-and-spoke network. *Ocean & Coastal Management*, 231, 106386.

Yu, H., Koga, S., Oliveira, T. R., Krstic, M., 2021. Extremum seeking for traffic congestion control with a downstream bottleneck. *Journal of Dynamic Systems, Measurement, and Control*, 143(3), 031007.

Zhang, L., Fu, L., Gu, W., Ouyang, Y., Hu, Y., 2017. A general iterative approach for the system-level joint optimization of pavement maintenance, rehabilitation, and reconstruction planning. *Transportation Research Part B: Methodological*, 105, 378–400.

Zhang, W., Jenelius, E., Ma, X., 2017. Freight transport platoon coordination and departure time scheduling under travel time uncertainty. *Transportation Research Part E: Logistics and Transportation Review*, 98, 1–23.

Zhao, X., Lin, Q., Yu, H., 2020. A co-scheduling problem of ship lift and ship lock at the Three Gorges Dam. *IEEE Access*, 8, 132893–132910.

Zhen, L., Shen, T., Wang, S., Yu, S., 2016. Models on ship scheduling in transshipment hubs with considering bunker cost. *International Journal of Production Economics*, 173, 111–121.

Zheng, J., Ma, Y., Ji, X., Chen, J., 2021. Is the weekly service frequency constraint tight when optimizing ship speeds and fleet size for a liner shipping service? *Ocean & Coastal Management*, 212, 105815.

Zhuge, D., Wang, S., Zhen, L., Laporte, G., 2021. Subsidy design in a vessel speed reduction incentive program under government policies. *Naval Research Logistics (NRL)*, 68(3), 344–358.